THESIS FOR THE DEGREE OF DOCTOR OF PHILOSOPHY

On Surface Characteristics and Microstructural Development of Soft Magnetic Composite Powder and Components

Christos Oikonomou

Department of Materials and Manufacturing Technology
CHALMERS UNIVERSITY OF TECHNOLOGY
Gothenburg, Sweden 2015

On Surface Characteristics and Microstructural Development of Soft Magnetic Composite Powder and Components

CHRISTOS OIKONOMOU

ISBN: 978-91-7597-279-4

Doktorsavhandlingar vid Chalmers tekniska högskola
Ny serie Nr 3960
ISSN: 0346-718X

Department of Materials and Manufacturing Technology
Chalmers University of Technology
SE-412 96 Gothenburg
Sweden
Telephone: +46(0)31-772 1000

Printed by Chalmers Reproservice
Gothenburg, Sweden 2015

To my family

and to all those who are next to me when I need them the most.

“Man! Enjoy! Whatever!”

- *Mister Kumar*

On Surface Characteristics and Microstructural Development of Soft Magnetic Composite Powder and Components

Christos Oikonomou

Department of Materials and Manufacturing Technology
Chalmers University of Technology

Abstract

Soft Magnetic Composite (SMC) products manufactured by traditional Powder Metallurgical (PM) techniques, are strong candidate materials for electromagnetic applications. Their advantages are based on cost and energy efficient production methods, shape complexity realization and uniquely uniform and isotropic three dimensional (3D) magnetic properties. SMC powder grades consist of individually encapsulated iron powder particles with an ultra-thin, electrically insulating surface coating. Component manufacturing procedure involves compaction of the admixed SMC base powder with a lubricant substance to a final shape, as well as a subsequent heat-treatment that aims at the relaxation of stresses induced during the compaction. The concept of SMC utilizes the insulating properties of the surface coating by creating a 3D laminated stack in a powder form, which essentially aims in a higher reduction of the total core losses of the application. In this manner, products with comparable or superior magnetic performances can be produced as opposed to the more traditional laminated steels and ferrites, especially for high frequency applications.

The electrical insulating coating, as well as the internal microstructure of the matrix powdered material, constitute two of the most important factors that control the final performance of an SMC product. Their state and its development through processing is crucial for tailoring the material to the desired properties. In the case of the coating, its morphology, thickness, cohesion to the powder surface and durability during compaction and annealing steps are all important aspects that contribute to the improvement of its functionality. Moreover, the degree of deformation, recrystallization and grain boundary interface related to the base material after treatment, are also heavily linked to its magnetic behavior. In the present study, methodologies along with theoretical modeling were developed initially based on analytical techniques, in order to assess and relate the aforementioned material properties to processing parameters such as compaction pressure, annealing temperature and composition of process atmosphere. For such purposes, both loose SMC base powder as well as compacted components were investigated before and after processing treatments in various conditions.

The results of this thesis address the nature of the insulating coating, in terms of chemical composition and microstructure, while pointing out the underlying mechanism responsible for its stability under heat treatment. Furthermore, the development of the deformation state and internal microstructure of the SMC processed components was assessed in respect to their processing parameters and correlated to their measured core loses. These findings are important contributions, especially from an industrial point of view, in achieving optimal properties for such composite materials as well as designing an efficient processing route. The methods and knowledge developed here can also prove to be of interest for a wider range of PM concepts.

Keywords: X-ray photoelectron spectroscopy, high resolution scanning electron microscopy, energy dispersive X-ray spectroscopy, electron backscatter diffraction, X-ray diffraction, focused ion beam, soft magnetic composites, powder metallurgy, surface layers, depth profiling, thickness determination, microstructure, annealing, compaction, magnetic testing

Preface

This PhD thesis is based on the work performed at the department of Materials and Manufacturing Technology at Chalmers University of Technology, between January 2011 and November 2015. The project has been carried out under the supervision of Associate Professor Eduard Hryha and Professor Lars Nyborg.

This thesis consists of an introductory part followed by the appended technical papers:

Paper I: Evaluation of the thickness and roughness of homogeneous surface layers on spherical and irregular powder particles
C. Oikonomou, D. Nikas, E. Hryha, L. Nyborg
Surface and Interface Analysis
Volume 46, Issue 10-11, pages 1028–1032, October-November 2014

Paper II: Development of methodology for surface analysis of soft magnetic composite powders
C. Oikonomou, E. Hryha, L. Nyborg
Surface and Interface Analysis
Volume 44, Issue 8, pages 1166–1170, August 2012

Paper III: Effect of Heat Treatment in Air on Surface Composition of Soft Magnetic Composite Components
C. Oikonomou, R. Oro, E. Hryha, L. Nyborg
Materials Science and Engineering: B
Volume 189, pages 90-99, November 2014

Paper IV: Effect of powder properties on the compressibility of water-atomized iron and low-alloyed steel grades
C. Oikonomou, E. Hryha, Å. Ahlin, L. Nyborg
Euro PM2013 conference proceedings, 15-18 September 2013

Paper V: Assessment of the compacting and annealing process steps on the performance of finished Soft Magnetic Composite components
C. Oikonomou, D. C. Gutiérrez, M. Monclús, J. M. Molina-Adareguia, L. Nyborg
Euro PM2015 conference proceedings, 4-7 October 2015

Paper VI: Assessment of thermal stability of inorganic electrical insulating surface layers in Soft Magnetic Composite materials by means of XPS
C. Oikonomou, E. Hryha, L. Nyborg
Submitted for publication at Surface and Interface Analysis special issue.

Papers not appended in this thesis

i. Application of EBSD analysis for strain depth profiling and microstructural evaluation of low-temperature carburized austenitic stainless steels
G. Maistro, C. Oikonomou, L. Rögstrom, L. Nyborg, Y. Cao
Submitted for publication at Surface and Interface Analysis special issue.

My contribution to the appended papers

I. Participated in the planning of the presented study. Performed part of the total experimental work and data evaluation. The first draft of the publication was written by the author and the final version in close collaboration with the co-authors.
II. Participated in the discussions of the presented study. Performed all the experimental work and data evaluation. The first draft of the publication was written by the author and the final version in close collaboration with the co-authors.
III. Participated in the planning of the presented study. Performed most of the experimental work and data evaluation. The first draft of the publication was written by the author and the final version in close collaboration with the co-authors.
IV. Participated in the discussions of the presented study. Performed part of the experimental work and data evaluation. The first draft of the publication was written by the author and the final version in close collaboration with the co-authors.
V. The author planned this study. Performed part of the experimental work and data evaluation. The first draft of the publication was written by the author and the final version in close collaboration with the co-authors.
VI. The author planned this study. Performed most of the experimental work and data evaluation. The first draft of the publication was written by the author and the final version in close collaboration with the co-authors.

A summary of contribution from my colleagues in the appended papers

I. The FIB measurements were performed by Dr. Yiming Yao using facilities in the Department of Applied Physics at Chalmers University of Technology. The source code and layout of the computer software was developed by Yaroslav Kish.
III. The XRD measurements were performed by Dr. Raquel de Oro Calderón in the Department of Materials and Manufacturing Technology at Chalmers University of Technology.
IV. All compaction testing was performed at Höganäs AB under the supervision of Åsa Ahlin.
V. The majority of the microscopy, magnetic testing and data analysis was performed by Daniel Castillo Gutiérrez in the Department of Materials and Manufacturing Technology at Chalmers University of Technology, as well as at Höganäs AB. The nanoindentation measurements were performed by Miguel Monclús and Jon Mikel Molina-Adareguia at IMDEA Materials institute in Madrid, Spain.
VI. The DSC measurements were performed by Assoc. Prof. Eduard Hryha in the Department of Materials and Manufacturing Technology at Chalmers University of Technology. The TGA measurements were performed by Mika Nilsson at Höganäs AB.

Table of Contents

List of acronyms

SMC	Soft Magnetic Composites
PM	Powder Metallurgy
XPS	X-ray Photoelectron Spectroscopy
EDX	Energy Dispersive X-ray Spectroscopy
HR SEM	High Resolution Scanning Electron Microscopy
EBSD	Electron Backscattered Diffraction
XRD	X-ray Diffraction
FIB	Focused Ion Beam
DSC	Differential Scanning Calorimetry
TGA	Thermogravimetry Analysis
BC	Band Contrast
LAGBs	Low Angle Grain Boundaries
HAGBs	High Angle Grain Boundaries
GNDs	Geometrically Necessary Dislocations
IPF	Inverse Pole Figure
AC	Alternating Current
DC	Direct Current
3D	Three Dimension (s/al)
SE	Secondary Electrons Detector
FSD	Force Scattered Detector
Inlens	Secondary Electrons In-lens Detector
WD	Working Distance
B	Magnetic Flux Density
H	Magnetic Field Strength
μ_{max}	Permeability
H_c	Coercive Force
B_s	Saturation Induction
P_h	Hysteresis Losses
P_e	Eddy Current Losses
P_r	Residual Losses
λ^{ox}	Attenuation length in surface layer
t^{ox}	Thickness of surface layer

1. Introduction

In this section, a brief description of Soft Magnetic Composite materials is given along with the thesis scope and goals for contributing to this field.

1.1. Background

Energy efficiency strategies have drawn much attention in the last decades, constituting a major part of the whole sustainable energy development effort. Nowadays, new policies for energy preservation are being introduced globally along with new legislations that target to the stabilization and reduction of the total CO_2 emissions in energy production, residential and commercial consumption, transportation and industry [1]. In this context, electromagnetic applications can prove to be beneficial if one takes into account the possibilities of their involvement in all of these fields. Power circuits, communication devices, microelectronics, automotive applications, household appliances and many more categories of contemporary utilities, all make use of the electromagnetic effect for energy storage and conversion [2]. Related to these phenomena though are energy losses, namely core losses, due to inherent material properties that reduce the efficiency of the applications by dissipating energy in the form of heat. Hence, the need for new improved materials for such type of purposes is constant and basically driven by an outgrowing consumption demand.

Soft magnets comprise the other most important family of ferromagnetic materials, along with the hard magnets, which are defined by their ease to magnetize and demagnetize even when subjected to low external magnetic fields. They have been being widely used as core for inductors and transformers in both DC and AC applications [2, 3]. Typically, steel laminated structures and ferrites are preferred due to their good electrical resistivity and high permeability. This attribute is essential in reducing the core losses by preventing the circulation of the deleterious induced eddy currents, especially at higher frequencies. The growth though of fields such as information technology, high frequency applications and electric motors increase the demand for more sophisticated technologies, which in turn push towards size reduction, minimizing energy losses and new complex designs that often test the limits of these more traditional solutions.

Promising alternatives to the latter are iron powdered cores, produced by compaction of individual electrically insulated iron particles under high pressures into compact solid forms. The idea behind this concept dates back to the 19^{th} century, though the advance in materials science and production techniques have given it a significant boost in the last decades. These materials, often termed as Soft Magnetic Composites (SMC), are being manufactured today by means of conventional powder metallurgical techniques [4, 5]. Their advantages lie in their isotropic nature and high electrical resistivity, which open up new design possibilities for weight, energy losses and reduction in production cost. Proper material selection and process treatment are hence important aspects that can further promote the flexibility of this technology in terms of applications. Today, the primary research volume related to the improvement of

SMC concept focuses on the development of more exotic and functional insulating materials, as well as various coating methods [6-8].

Thus, in order to contribute to this effort, the development of robust analysis methods can be proven crucial in delivering fundamental knowledge and tools for further understanding and development of the materials in question.

1.2. Scope and Goal of this Thesis

As mentioned earlier one of the main advantages of the SMC products is their significantly reduced energy losses, especially at high frequency applications, as compared to their laminated steel or ferrite counterparts. This can be mainly attributed to the presence of an electrically insulating coating that encapsulates and separates each individual metal particle in the component. The processing stages followed at the production of such materials, i.e. compaction and annealing steps for shaping and stress relief purposes respectively, influence heavily the final properties and performance of these composites [9, 10]. It is possible that such type of operations might have an adverse impact on the quality of a SMC component, by negatively affecting both the integrity of the insulating coating and by altering the characteristics of the base material. Thus, the viability of the surface layer, as well as the microstructural development in the base powder and degree of plastic strain stored in the latter are all key parameters that need to be taken under consideration and be assessed.

The scope of the present thesis is to investigate from a materials science perspective the effect of such processing steps to the nature the SMC material, by unveiling all those mechanisms involved in every stage and their contribution to the final result. By increasing the knowledge in this context it is possible to further develop and optimize both the process and the material for improved performance.

In order to achieve this, the goals were set to develop the necessary methodologies that would allow the investigation of the effect of processing steps to the properties of the material of interest. For such purposes initially a methodology was built based on analytical techniques that would enable the evaluation of the homogeneity, chemical composition *vs* depth and thickness of the insulating coating. To that end, a theoretical model was additionally developed and implemented for thickness determination of the surface layer using surface sensitive analytical techniques. Based on such methodology, the effect of the heat-treatment was investigated and its influence on the state of the insulating coating was evaluated. Moreover, a second methodology was developed for assessing the microstructural evolution and deformation state of the base powder material during compaction and annealing operations. This method was implemented on processed components treated under different conditions. Finally, the last goal of the thesis was set to investigate the magnetic performance of the SMC parts and correlate it to the findings from the aforementioned investigations.

2. Soft Magnetic Materials

In this section of the thesis, a brief introduction to the soft magnetic material is given, including their classification based on their composition, properties and applications.

2.1. Overview

Both ferro- and ferrimagnetic materials have been generally divided into two large families, namely soft and hard magnets, based on their ease to magnetize and demagnetize under an applied field [11]. Differences between them can be better illustrated by examining their hysteresis loops when subjected to a magnetization cycle under an externally applied magnetic field, as shown in Figure 1. In the case of a soft magnet, saturation is easily achieved even under fields of low strength which is not the case for a hard magnet.

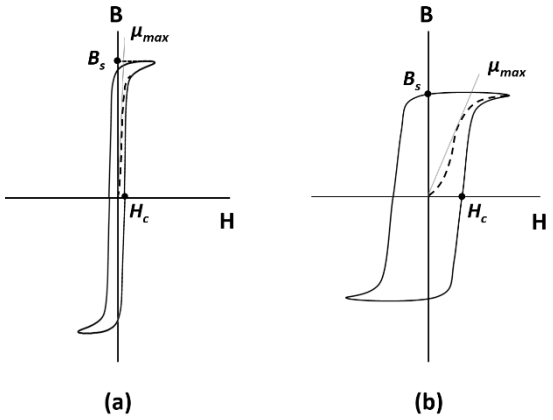

Figure 1: Hysteresis loops for (a) soft and (b) hard magnetic material.

It can be observed that for a material to be soft magnetic, its hysteresis loop should be as thin and extended as possible. This translates to a low value of the coercive force of the material (the amount of the reverse applied field H_c that is needed to decrease the induction to zero), high value for its magnetic permeability μ_{max} (a measure of its magnetic sensitivity defined as B/H), and high saturation induction value, B_s.

Since hard magnetic materials are difficult to demagnetize, the energy stored in them and expressed as an external magnetic field will last indefinitely (or until an external source causes them to demagnetize). For this reason, they are used in applications where permanent magnets are required such as magnetic recording, memory devices, motors, speakers and sensors, among others.

On the other hand, the ability of the soft magnets to easily magnetize and demagnetize renders them ideal candidates for both AC and DC applications. Thus, they are widely used as cores in transformers and inductors in order to enhance and/or channel the produced magnetic flux [2, 3, 11].

2.2. Core Losses

The dissipation of energy in a magnetic core during its magnetization and demagnetization cycle is widely termed as core losses. While these are not of high importance for hard magnets, they are crucial in the efficiency of soft magnetic applications and can be controlled with proper material selection [3, 4, 11]. Core losses are generally divided into three categories, namely hysteresis losses (P_h), eddy current losses (P_e) and anomalous losses (P_r).

The hysteresis losses originate from the movement of the domain walls back and forth under a magnetization/demagnetization loop. The presence of impurities, precipitates, imperfections, grain boundaries and dislocations act as barriers towards this motion and increase those losses. These can be measured from the internal area of the hysteresis loop and exhibit a linear relationship with the frequency of the applied field.

The eddy current losses, alternatively named classical eddy current losses, are caused by the existence of stray electric currents that circulate into the bulk of the material. The subjection of a magnetic material to a fluctuating magnetic field induces swirling currents in rotating patterns that eventually dissipate energy in the form of heat. Classical eddy currents are considered macroscopic and become extremely important in high frequency applications due to their squared relationship with the latter.

The residual losses, also called anomalous losses or excess eddy current losses, are dynamic losses related to the circulation of the eddy currents due to domain wall motion but on the microscale [12, 13]. These are also material dependent and escalate with increasing frequency, but their contribution is indirectly measured from the difference of theoretical and experimental results.

2.3. Materials and Applications

In industrial soft magnetic applications, the ferromagnetic elements Fe, Co and Ni along with soft ferrites (i.e. ceramic compounds based on iron oxides with the addition of mainly Ni, Zn and/or Mn), are the most important families of materials. They exist in different alloyed compositions and produced under various fabrication techniques in order to achieve the best ratio of performance and cost for a specific application. For example, iron-cobalt alloys are known as the materials with the highest saturation flux values but also for being very expensive, as compared to pure iron or iron-phosphorus products which have good induction values and low cost. Iron-nickel alloys on the other hand have the highest permeabilities while the iron-silicon system is extensively used for its low coercive force and good resistivity. These materials are mainly being manufactured either in the form of laminates stacks or as powder-based cores depending on the designed application. In the first case, metal strips produced by different forming processes are joined together, while in the second case insulated iron particles are used as base material in finished products via mild sintering operations or by using various types of binder substances, i.e. bonded magnet cores. In addition to these concepts, nowadays

the development of iron based magnetic materials in amorphous and nano-crystalline states by liquid quenching techniques is favored due to their low coercive force and high resistivity. Soft magnetic materials, as described earlier, are used typically for core applications in transformers, inductors, actuators, chokes, filters, sensors, detectors and contractors among others, in order to enhance and/or channel the produced magnetic flux.

In **Error! Reference source not found.** some of the most commonly used soft magnetic aterials are mentioned along with representative production techniques and applications.

Table 1: General classification of soft magnetic materials based on their composition, production techniques, properties and applications.

Alloys	Production Techniques	Properties	Applications	References
Pure Fe	Powder-based (SMC/sintered)	good saturation flux /low cost	filters/pure inductors /power transformers /sensors/actuators /electric motors	[2-4, 14-16]
Fe-P	Powder-based (sintered)	good saturation /good mechanical properties/low cost	pure inductors /power transformers /rotary actuators/sensors	[2, 4, 17, 18]
Fe-Si	Laminated /Thin tapes /Powder-based (sintered)	good electrical resistivity /stability with age /good mechanical properties/low cost	pure inductors /power transformers /relays/solenoids	[2-4, 15, 17, 18]
Fe-Ni	thin tapes /powdered (sintered)	high permeability /low flux density /high cost	pure inductors /power transformers /actuators/detectors /sensors/contractors	[2-4, 15, 17, 18]
Fe-Ni-Mo	Powder-based (sintered)	high permeability /stability with time and temperature /high cost	loading coils/filtering coils/switching power supplies	[2, 3, 15]
Fe-Co	Laminated /Powder-based (sintered)	high saturation flux/high cost	actuators/ aerospace motors/ high performance transformers/filters	[2, 4, 15, 17]
Soft ferrites	Laminated /Powder-based (sintered)	high resistivity /low saturation flux /low cost	power transformers/filter inductors/sensors	[2, 3, 15, 17]
Fe-B-Si	Laminated /Powder-based	high magnetic permeability /good saturation flux / high resistivity	high frequency aerospace transformers	[2, 3, 19, 20]
Fe-Co-Si				
Fe-Cu-Si				
Fe-C-P-B-Si-Mo				
Fe-B-Si-Nb				
Fe-P-B-Si				

3. Soft Magnetic Composites

In this section of the thesis, the concept soft magnetic composite materials is presented along with information on their processing and treatments.

3.1. Overview

Development of soft magnetic products for electromagnetic applications produced by conventional powder metallurgical techniques is a continuous growing field [2, 4, 5, 12, 14-18, 21]. These can be generally divide into two families, the ones produced by sintering of the base powder material into finalized components and the ones for which sintering is avoided but the bonding is facilitated by the presence of various types of binder materials. To the first family belong the iron based alloys described in the previous section which are targeted for DC applications of less than 50Hz, exhibiting high saturation flux and good mechanical properties [4, 18, 22]. The second family, which is known as Soft Magnetic Composites (SMC), considers powder-based parts that consist of individually encapsulated iron particles with an electrically insulating coating, bonded together in three dimensional structures (Figure 2) [5, 16, 21].

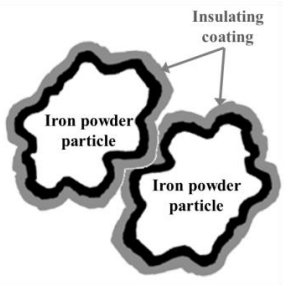

Figure 2: The SMC concept.

The advantages of using the SMC technology for electromagnetic applications are illustrated in Figure 3.

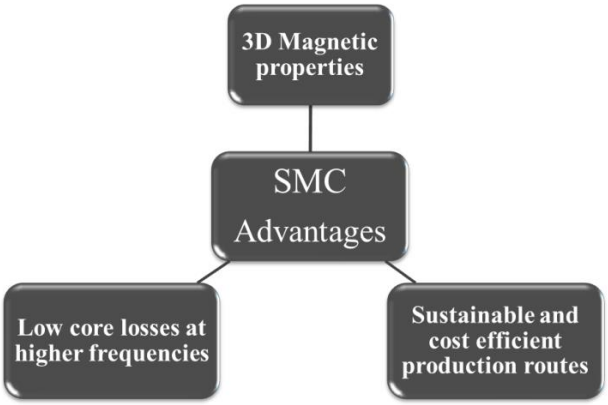

Figure 3: Advantages of the SMC technology.

The concept of the SMC aims at reducing the core losses in a component by introducing higher bulk resistivity through the increased insulating interfacial volume. The later can be tailored to the application of interest by varying the iron particle size and/or the thickness of the insulating coating. In this manner, the SMC technique offers a unique combination of magnetic saturation and resistivity levels, and consequently higher flexibility in terms of applications range as compared to the more traditionally used laminated steels and ferrites (Figure 4).

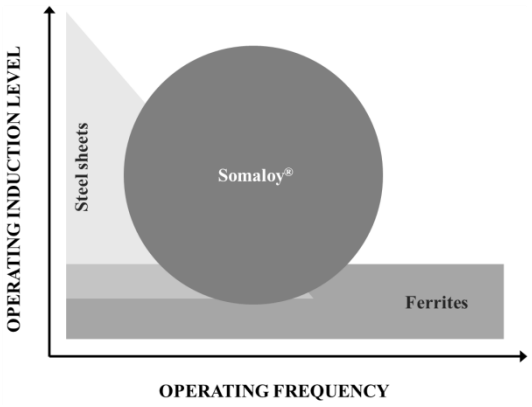

Figure 4: SMC positioning among laminated steels and ferrites in electromagnetic applications. Redrawn from [16]

Another attractive advantage of the SMC concept lies in the fact that new design possibilities open up due to the isotropic nature of SMC components. Unlike the laminate steels, SMC products can then make use of their ideally three dimensional (3D) flux capabilities. Innovative and more sophisticated applications of higher complexity can now be realized, that lead to reduced size products and less copper windings necessary [14].

Moreover, the SMC products prove to be an appealing option for electromagnetic applications due to their potentially low production cost. Taking full advantage of the well-established manufacturing techniques offered by Powder Metallurgy (PM) industry, it is possible to manufacture 3D-net-shaped components with high tolerances, property consistency, ease in recyclability and efficient material utilization in large volume production [4, 5, 14].

3.2. Insulating Coating

The insulating coating that separates the individual iron particles in an SMC product is the paramount feature of this technology. Its thickness, coverage and endurance under the different processing operations are key aspects to the properties of a magnetic part. The insulating coating can serve dual purpose in a SMC component, that of increasing its bulk electrical resistivity and/or acting as a binder substance to improve its mechanical behavior. In general, these coatings can be divided into two large families, namely organic and inorganic based [4]. Most common methods for applying such surface layers on powder materials are either immersion baths, sol-gel methods or through oxidation during annealing in the case of inorganic coatings. Dissolving, mixing and drying, polymer substances in solvents with subsequent

polymerization on the powder surfaces are the most preferred routes for organic coatings [6-8, 23-26].

The latter have been used extensively in processing of powder-based cores and can be divided into thermosetting and thermoplastic categories [4]. These approaches are preferred owing to the fact that they can act as binder medium and introduce acceptable mechanical strength to a part, though they cannot be used in too large volumes due to the reduction in permeability that they impose. A significant drawback for the use of organic coatings is their limited thermal stability, especially for thermosetting resins. This does not allow such SMC parts to be adequately stress relived at sufficient high temperatures for the reduction of hysteresis losses [24]. On the other hand, thermoplastic resins offer improved stability, but have worse surface coverage of the powder particles due to the difficulties in handling and processing.

The most common type of inorganic coatings used in the SMC technology are the phosphates (Zn/Fe/Mn), followed by oxides and sulfates [4]. Phosphatizing is a well establish metal conversion method and it has been used extensively in the steel industry [27]. The robust application methods for large-scale volume productions render these coatings ideal for industrial usage. Phosphate-based coatings possess an attractive combination of properties by providing good electrical insulation, anti-corrosive properties, thermal stability and can be functionalized and upgraded to more complex and improved structures [7, 8, 25, 26, 28].

3.3. Processing of SMC Materials

An SMC part has to go through different processing steps in a production line in order to acquire the desired final shape and properties. It should be understood that the combination of the base material and respecting processing parameters provides with a range of properties that can be tailored specifically for a desired application. It is obvious that these two are linked and the behavior and properties of the selected materials under the different processing steps will dictate the limits of the SMC concept.

The manufacture of an SMC part via conventional PM production techniques starts with the base material selection. In most cases pure iron or low alloyed iron-based powder containing Si, Ni, Al or Co and of various particle size distribution are used, which are typically produced by means of water atomization techniques [4, 5]. These powders are subsequently coated with the insulating surface layer, mixed with a lubricant and/or binder system, compressed under uniaxial high pressure (usually up to 800 MPa) to net-shaped bodies and then finally subjected to post heat-treatment process, typically between 220 - 700°C [4].

The importance of the particle size, insulating coating and binder system to the properties of an SMC part were mentioned earlier. The effect of lubricant is also important for the performance of a finished SMC component, since it reduces inter-particle and particle-to-die-wall frictions during the compaction process, which can be proven detrimental to the coating quality. The downside of lubricant usage though can be that by-products produced during its burn-off stage in the heat-treatment process, could also affect the nature of the coating by locally creating

strong reducing atmospheres [9]. Moreover, an increased volume of the lubricant will improve the resistivity of the component, but has an inverse effect on its permeability and maximum flux density [12].

In the compaction process the SMC components are brought to their final shape in one step, which consists a very cost efficient route. Through this process higher density values are targeted which are essential for achieving high induction. The process though introduces plastic strain to the bulk of powder grains, as well as gives high probability of damaging the insulating layer. These effects increase the core losses of the component substantially by increasing the hysteresis and eddy current losses, respectively [4, 12]. Different compaction techniques can be applied in order to get optimum results with respect to shaping, densification and minimizing impact on powder bulk and layer characteristics. These include warm compaction (where both the powder and the tool are heated), room temperature compaction, controlled die temperature compaction (where only the tool is heated up), two step compaction and high velocity compaction [4, 10].

To minimize the effect of the strain introduced into an SMC component during its compaction, for improving its properties, a post-compaction heat-treatment step is required. In some cases, this step is required for curing purposes if a binder system is added, usually at lower temperatures [24]. The stress relief is a time-temperature related phenomenon and in principle, higher temperature regimes or longer dwelling times are needed for better tuning the properties of SMC components. The time-temperature recipe for a heat-treatment, as well as under which type of processing atmosphere this should take place, are largely dependent on the viability of the insulating layer during this step [9, 10]. It is thus crucial that in the SMC concept no sintering and no deterioration of the coating should take place, since that would mean that electrical short cuts between powder particles will exist yielding finally higher eddy current losses.

4. Materials and Experimental Details

To fulfill the goals of this thesis various analytical techniques were utilized complementary, along with mechanical and magnetic testing. A detailed description is presented in the current section regarding the materials investigated, the experimental details related to the implementation of the related techniques and the methods used for such purposes. The schema provided below in Figure 5 outlines the experimental procedure followed in this thesis in every step. Information regarding the techniques mentioned in this section of the thesis is provided below in the "Analytical Techniques" chapter.

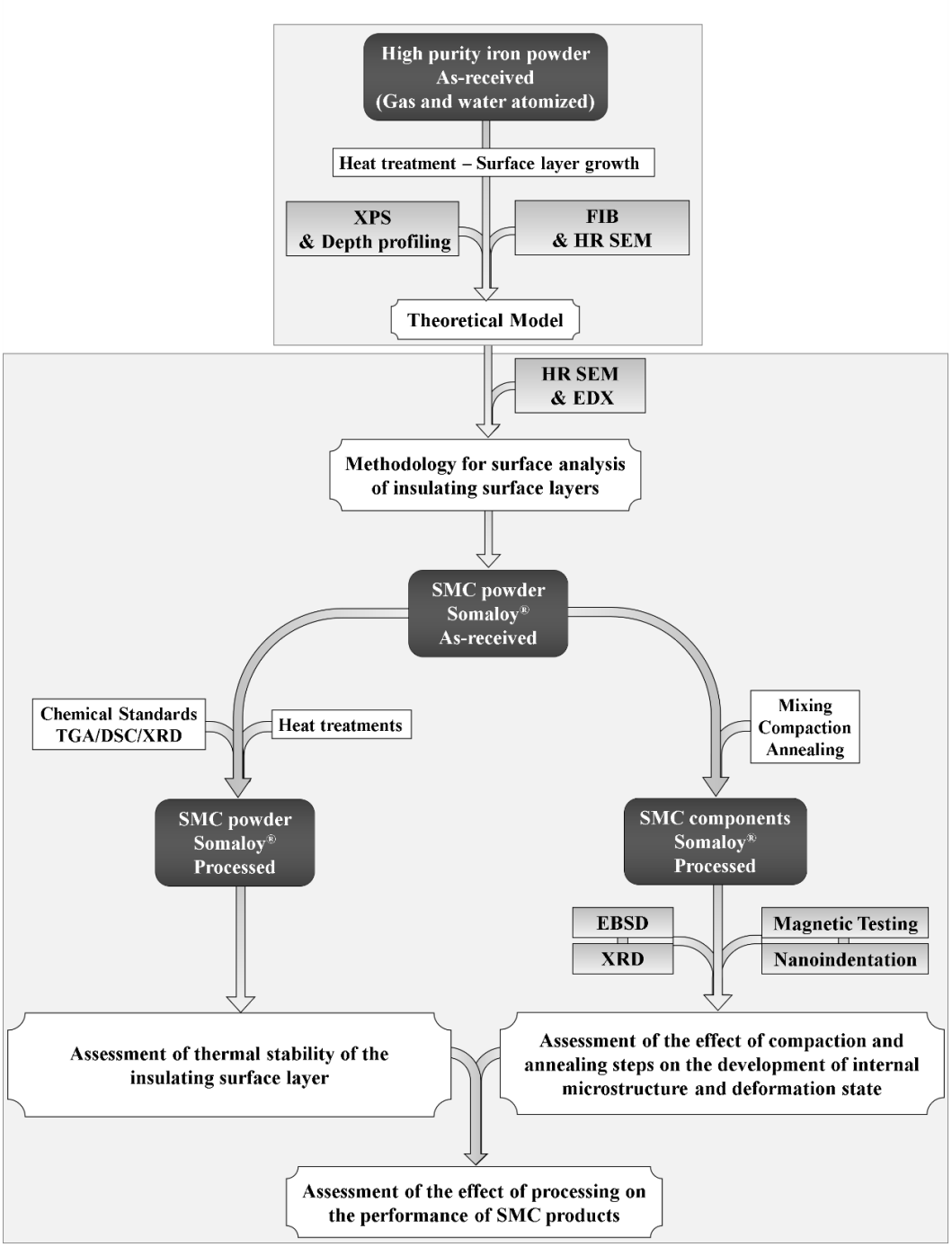

Figure 5: Schema of experimental investigations.

Initially a theoretical model based on XPS technique coupled with depth profiling by ion etching was developed and implemented on high purity iron grades of spherical and irregular shape. In this study, complementary analytical techniques such as HR SEM and FIB were utilized along with XPS analysis in order to experimentally verify the validity of the model. Subsequently, a methodology was developed and implement on SMC grades based on HR SEM, EDX and XPS analytical techniques for investigating the chemistry and morphology of their insulating layer. This methodology was later utilized in order to assess the thermal stability of the surface layer on SMC loose powder and components under different temperature regimes and processing atmospheres. For such purposes chemical standards of high purity were analyzed in similar conditions as references, while additional techniques such as DSC, TGA and XRD were implemented in a complementary manner. Finally, a methodology based on HR SEM, EDX, EBSD and nanoindentation techniques was presented and implemented for assessing the development of internal microstructure and deformation state of powdered products. The results from such type of analyses on SMC components were further correlated to their magnetic properties in order to assess their performance from a materials science point of view.

4.1.Materials

4.1.1. Plain and pre-alloyed iron powder grades

Pure iron powder produced by means of water and gas atomization at Höganäs AB, Sweden, were utilized for the experimental needs of the theoretical model development in Paper I. These grades have been characterized elsewhere in relation to their morphology, surface characteristics and chemistry [29]. The water atomized powder exhibits a characteristic irregular shape as opposed to the spherical one of the gas atomized, while in both cases it was established that the powder surface was largely covered by a homogeneous iron oxide layer of less than 10 nm in thickness. In the presented study, both grades were subjected to further oxidation by heat treatment in air at 300°C prior to the analysis. This treatment was necessary in order to grow sufficiently thick surface oxide layers reaching above the $3\lambda^{ox}$ limit (λ^{ox} is the electron mean free path in the oxide layer) that is desirable for implementing the depth profiling technique in the X-ray photoelectron spectroscopy (XPS), as well as to cope with the resolution limit of the high resolution scanning electron microscopy (HR SEM) technique. In addition, both kinds of powder were sieved into a particle size fraction of 28-53 μm to minimize any shading effects imposed by the particle roughness during the XPS investigation. The same powder fraction was also examined with focused ion beam (FIB) and HR SEM for consistency purposes.

For assessing the compaction behavior and internal microstructure of powdered products in Paper IV, in addition to the high purity water atomized powder an iron pre-alloyed powder grade with 3 wt. % chromium and 0.5 wt. % molybdenum produced by Höganäs AB, Sweden, was used. The pre-alloyed powder, also produced by water atomization process, has been extensively characterized elsewhere [30]. Both grades were sieved down in to four fractions

(<45 μm, 45-71 μm, 71-104 μm and >104 μm) for the needs of this study and compacted by uniaxial die pressing at different pressures between 100 and 800 MPa. The powders were admixed with 0.5 wt. % of organic lubricant prior to their pressing.

4.1.2. Somaloy® material

The commercial SMC powder grade Somaloy® produced by Höganäs AB, Sweden, was used as reference material for the studies presented in Papers II, III, V and VI. It consists of high purity water-atomized iron powder with particle size less than 150 μm, coated with an ultra-thin inorganic electrically insulating surface layer as described by a patented process [23]. The powder was analyzed both in as-received form as well as in processed SMC components having toroidal ring shape of 5x5 mm cross section and outer/internal diameter dimensions of 55mm/45mm, respectively. The production of these components for Papers III and V included admixing the SMC powder with 0.5 wt. % of commercial organic lubricant Kenolube™, compaction under conventional uniaxial die pressing at 800 MPa and heat treatment in air for 30 min, including de-lubrication and stress relief steps, at temperature regimes of 400, 500, 550, 600 and 650°C depending on the study. The heat treatment of the as received SMC powder in Paper VI was carried out in both oxidizing (air) and inert (N_2) processing atmospheres with 20 min holding time at the temperature of interest.

4.1.3. Chemical standards

The high purity powdered chemical standards of iron (III) phosphate di-hydrate ($FePO_4 \cdot 2H_2O$) and di-phosphorus pentoxide (P_2O_5), that were investigated in Paper VI, were purchased from Sigma-Aldrich®. In the presented study, these compounds were processed and analyzed under similar conditions as the SMC powder grade.

4.2. Analytical Techniques

4.2.1. X-ray Photoelectron Spectroscopy

X-ray Photoelectron Spectroscopy (XPS) is a surface sensitive analytical technique that provides chemical compositional and chemical state information of the investigated material from a very small analysis depth of the order of few nanometers into the surface [31, 32]. Combined with ion etching technique it is possible to achieve depth profiling of the sample of interest. These attributes of XPS as well as its sensitivity to chemical environment changes (chemical peak shifts) and wide range of type of materials that can be examined makes it very appealing for surface and interface analysis in material science [33].

This technique has been used extensively for analysis of flat surfaces [32, 33] with an enormous amount of experimental methods and modeling efforts now available to the researcher. On the contrary, it has not been so popular for investigating surfaces of specific geometry and roughness due to the anticipated shading effects from such samples and the subsequent

uncertainties that these bring to the results. Previously, a theoretical model for analyzing spherical particles using depth profiling technique combined with XPS was developed and experimentally tested by Nyborg et al. [34]. In their study, the effect of the surface geometry of the sample on the photoelectron intensity, X-ray flux and ion sputter rate was formulated for a specific experimental arrangement. By doing so, it was possible to evaluate the thickness of a homogeneous surface layer on a powder sample with a core-shell structure using depth profiling and by taking into account the normalized intensity of the substrate material at a certain relative metallic intensity fraction, defined by the relationship of the thickness of the layer over its attenuation length.

In this thesis, the XPS technique has been implemented for further developing the theoretical model and also to investigate the surface chemistry of the SMC powder in as-received state and finished components. In all cases a PHI 5500 (PERKIN ELMER, Eden Prairie, Minnesota, USA) instrument was used for analysis, equipped with a monochromatic Al K_α (1486.6 eV) X-ray source under ultra-high vacuum (UHV) conditions ($1x10^{-12}$ bar). In the current experimental setup both the X-ray source and spectrometer axis formed a 45° angle with respect to the sample surface normal direction, as well as to the normal of the sample surface, while the ion gun was positioned at 50.5° from the sample surface. A schematic representation of this arrangement can be seen in Figure 6.

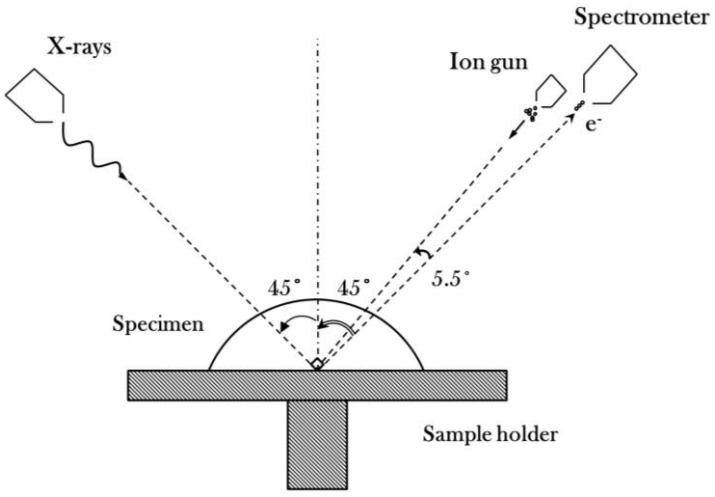

Figure 6: Experimental arrangement for XPS in current thesis.

Prior to the analysis, instrument calibration was performed using pure elemental standards (Au $4f_{7/2}$:84.00 eV, Ag $3d_{5/2}$:368.3 eV, Cu $2p_{3/2}$:932.7 eV). Additionally, ion etch rate calibration was carried out on a flat oxidized tantalum foils (Ta_2O_5) of known thickness (100nm) yielding an etch rate of 21.6 Å min^{-1} over a rectangular area of $3x4mm^2$ at 3 kV or 50 Å min^{-1} over the same area at 4 kV ionization voltage. For all high resolution (HR) spectrum analyses, 23.5 eV pass energy and 0.1 eV/step were used while for all survey scans 93.9 eV and 0.4 eV/step, respectively. The analyzing area was approximated at 0.8 mm in diameter in all cases, which means that more than 100 particles being analyzed at the same time.

The heat-treated SMC components where fractured prior to their analysis and both outer and center regions of their cross sections were examined. The analyzed powder samples where loosely mounted on double adhesive conductive carbon tape (C1s: 285.1 eV) in order to prevent any further deformation of the particles and ensure the integrity of the surface layers. The detected carbon signal was used as a reference value for charge compensation purposes. Due to the high purity of the analyzed materials, carbon signal was attributed to the existence of adventitious hydrocarbons on the samples surface, both for components and as-received powder. Charge compensation was performed in all cases using software correction and a low energy electron charge neutralizer flood gun. For greater etch depths, where needed, the signal of the metallic iron was also used as a reference for charge peak shifting correction. The analysis and curve fitting of the collected spectra was performed with a PHI Multipak (Physical Electronics) software and for this an asymmetric Gaussian-Lorentzian line shape was preferred combined with Shirley background subtraction [33].

4.2.2. High Resolution Scanning Electron Microscopy – Energy Dispersive X-ray spectroscopy

For the needs of surface morphology characterization, for both powder samples and components, high resolution scanning electron microscopy (HR SEM) was implemented using a LEO Gemini 1550 (CARL ZEISS - LEO electron microscopy, GmbH, Germany) electron microscope equipped with a field emission gun. An in-lens secondary electron detector built in the electron column of the microscope was preferred for such type of analysis due to its high sensitivity at close working distances and low acceleration voltages, providing superior topographic and material work function related information with high lateral resolution. Energy dispersive X-ray spectroscopy (EDX) was also utilized as means of complementary chemical microanalysis in Papers II and III with an INCAEnergy system, though due to the inherent surface roughness of all samples the results can only be evaluated qualitatively. Calibration for the microanalysis was conducted using elemental standards of cobalt for 20, 15 and 10 kV and silicon for 5 kV. All powder samples were soft pressed into aluminum plates for HR SEM and EDX analysis while no special preparation was needed for the fractured surfaces of the components.

4.2.3. Electron Backscatter Diffraction

Electron backscattered diffraction (EBSD) is a characterization technique embedded in the SEM which can be utilized for microstructural evaluation of crystalline or polycrystalline materials, providing information on grain orientation, point-to-point orientation relationships, texture analysis and phase identification [35]. In addition to the microstructural evaluation, the EBSD technique has become extremely popular in materials science for investigating plastic deformation and performing strain analysis based either on the degradation of the diffraction patterns in strained materials, or on the local misorientation between analyzed points [36, 37].

For such type of analyses matter is probed by an electron beam of specific energy and the diffraction events occurring at its surface from various crystallographic planes are being detected, processed and identified by specialized electronic systems and computer software [38]. Specimens are usually positioned tilted at 70° in vacuum conditions in the SEM chamber for increased yield of backscattered electrons and improved contrast in the diffraction patterns. Experimental parameters such as working distance, acceleration voltage, beam current density and step size are known to influence the outcome of the measurements and should be optimized based on the strength of the current microscope and material under investigation [35]. Additionally, an adequately smooth sample surface is required in order to ensure the quality of the diffractions pattern detected and analyzed by the technique. Sample preparation methods can vary between mechanical polishing, electropolishing, ion milling and plasma etching depending on the material under investigation.

In Papers IV and V, both loose powder and cross sections of the processed components analyzed by EBSD were mounted in conductive resin (PolyFast by Struers). The samples were mechanical polished down to 1 μm with diamond suspension, followed by an oxide polishing step with silica suspension (OPU by Struers). For EBSD analysis a step size of 0.5 μm was used for single powder particle analysis and 1 μm for large area mapping. The working distance (WD) for all measurements was set between 15 and 20 mm and the acceleration voltage of the electrons at 20 kV. For the case of the processed components a total area of 0.7 mm^2 was analyzed for all conditions from three different samples. All EBSD maps were collected with a Nordlys II detector (Oxford Instruments, High Wycombe, England) incorporated in the SEM system. The data evaluation from all measurements was performed with Channel 5 software from HKL Technology Inc. (Hobro, Denmark).

4.2.4. Focused Ion Beam

The focus ion beam (FIB) technique in combination with HR SEM were used in Paper I in order to determine the homogeneity and thickness of the surface layers from both gas and water atomized powder grades. The synergy of these techniques provides the user with the opportunity of performing in-depth analysis on sub-surfaces from exposed cross sectional regions created through a series of cutting and imaging of the material. This is achieved by having a dual beam system focused on the sample, consisting of an ion beam for sputtering and electron beam for imaging purposes. In this thesis a FEI Versa 3D DualBeam FIB–SEM station was used, equipped with a field emission gun (FEG) source and gallium high-current liquid metal ion source. Prior to the ion sputtering operations the samples where first gold coated with an Edwards Sputter coater S150B before they were introduced to the station. Subsequently, a platinum layer of 2 μm thickness was deposited on the site of interest *in situ* with an Omniprobe micromanipulator needle in order to protect the surface layer and achieve a sharp interface. The ion sputtering was carried out with gallium ions of 2 to 30 keV energy and 27 to 65000 pA beam current until the desired cross sectional surface quality was exposed. The samples were prepared by soft pressing the powder grades into aluminum plates similarly to the HR SEM analysis.

4.2.5. X-ray Diffraction

In the present thesis, the X-ray diffraction technique was used for phase identification analysis at different temperature regimes of the high purity chemical standards in Paper VI and for the exterior surface of the SMC heat-treated components in Paper III. The experimental measurements were carried out using a Bruker D8 ADVANCE diffractometer equipped with a Cr-Kα source using 0.05° 2θ/step and 5 sec/step conditions for all measurements. In Paper VI the analysis was carried out in a Bragg-Brentano theta-theta configuration for $10° < 2\theta < 140°$, while in Paper III it was conducted under grazing angle mode at an incident angle of 3 degrees over a range of $40° < 2\theta < 140°$. All phases present were identified based on the PLU2013:340653 database, while the penetration depths of the X-rays for the compounds of interest were calculated with the AbsorbDX V.1.1.4 software.

4.2.6. Thermal analysis

Thermal analysis by means of differential scanning calorimetry (DSC) and thermogravimetric analysis (TGA) was conducted in Paper VI for evaluating the thermal characteristics, such as stability and structural transformations of the high purity chemical standards. For such purposes a STA 449 F1 Jupiter thermal analyzer from Netzsch was utilized in both air and N_2 atmospheric conditions with a heating rate of 10 °C/min.

4.2.7. Nanoindentation

Mechanical testing by nanoindentation technique was performed in Paper V on processed SMC components as part of the development of a methodology for evaluating their deformation state. The technique measures the hardness of the material on a submicron scale by measuring the depth of penetration under an applied load of an indenter of well know geometry, a three-sided Berkovich indenter in this case. As opposed to conventional macro or micro hardness testing nanoindentation can be considered as a form of non-destructive technique, since the defects produced on the surface of the material are negligible. Additionally, it offers the possibility to investigate residual stresses or discrete events such as recrystallization and phase identification [39, 40]. The nanohardness values can be extracted from a load-displacement curve, which is obtained by measuring the force and displacement of the indenter when subjected to a prescribed loading and unloading profile during the nanoindentation test [41].

The nanoindentation tests in the present thesis were performed with a Triboindenter TI 950 (Hysitron Inc., Minneapolis, MN, USA) in displacement control testing mode, at an imposed maximum depth of 200 nm using a Berkovich type diamond indenter. Loading, holding and unloading times of 10, 5 and 5 sec respectively were implemented that yielded maximum applied forces in the order of 2 - 3 mN. Each nanoindentation map consists of an array of 10 time 10 indents with 5 μm spacing between them in both vertical and horizontal directions.

4.2.8. Magnetic testing

In order to correlate the findings of this thesis to the performance of the SMC products, resistivity and magnetic testing in both AC and DC conditions were performed in Paper V. The resistivity test evaluates the bulk electrical resistivity of the material and was carried out with a simple four-point-measurement setup, operating with a constant current source while measuring the voltage from four different contact point couples. The formula for calculating the measured resistivity is given below:

$$\rho = \frac{Average(V1,V2,V3,V4)\cdot 2\cdot A}{I\cdot l} \qquad (1)$$

In equation (1) the resistivity is expressed in Ohms·m, the voltages at mV, the cross section area A of the test ring in cm^2, the current intensity I in mA and the length between the two measured contact points in cm.

The DC and AC tests were performed with a Brockhaus Messtechnik equipment in order to evaluate with the former the maximum permeability, coercivity and hysteresis losses and with the latter the eddy current losses. All test rings were coiled prior to their measurement with an interior and an exterior copper winding of 100 turns each, acting as drive and sense windings, respectively. In DC conditions the strength of the external field was set at 10000 A/m, while in AC conditions three levels of induction were implemented namely 0.5 T, 1 T and 1.5 T at frequencies from 50 Hz up to 1000 Hz.

5. Results and summary of appended papers

In this section of the thesis the results and a summary of the appended papers are given, along with key discussion points and some complementary material to better illustrate all of the findings. In Paper I, the further development of the existing theoretical model [34] for estimating the thickness of homogeneous surface layers on spherical shaped particles using depth profiling technique with XPS was presented. The model's formulation was introduced and its validity was experimentally assessed using XPS on pure iron powder grades of regular and irregular morphologies. Additional analytical techniques such as FIB – HR SEM were also implemented for validation of the model. In Papers II and VI SMC powder in both as-received and annealed states, respectively, were analyzed. In the first case a methodology was developed based on XPS, HR SEM and EDX techniques for chemical, topological/morphological and depth profiling analysis of such type of insulating layers. Different sample preparation and charge compensation methods were tested and optimum conditions for imaging and chemical analysis were established. In the second case, the SMC powder was heat-treated under various conditions and investigated using HR SEM, EDX, XPS, XRD and DSC/TGA techniques. The effect of the temperature and atmosphere composition on the thermal stability of the surface insulating coating was evaluated. In Paper III, processed SMC components were studied after being annealed at different temperature regimes. The methodology established previously for SMC powder was implemented and the effect of processing conditions on the surface characteristics of the products at different regions was assessed. In Paper IV, a methodology based on combining HR SEM, EDX and EBSD techniques for investigating the internal microstructure of powder materials was introduced. In Paper V, this methodology was further developed by correlating EBSD results with nanoindentation measurements to assess the degree of mechanical deformation in powder compacts. Subsequent investigations, based on the aforementioned approach, were conducted on SMC powder and processed components under various compaction and annealing conditions. The effect of the processing stages on the microstructural development of SMC materials was evaluated and related to their performance through magnetic testing in Paper VI.

5.1. Theoretical model development for layer thickness determination on powder materials

For samples of specific geometry and roughness the experimental arrangement, as described in section 4.2.1., can influence the result of an XPS depth profiling measurement. In these cases, as opposed to flat surfaces, inherent shading effects can be introduced and affect the analysis due to their irregular morphologies. Additionally, the X-ray flux, photoelectron intensity and ion sputter rate are not constant over the whole analyzed surface area when probing such type of surfaces, as it exhibits an angular dependency with respect to the angle of ion incidence [32, 42]. In particular, such type of dependency in ion etching results in non-homogeneous material removal over the probed area. This is due to the fact that the positioning of the ion gun in space with respect to the spectrometer and to the X-ray source will dictate the amount of residual layer that will be analyzed. In Figure 7 an attempt to illustrate this effect is shown for a

hypothetical spherical core-shell structure (the dashed interior yellow sphere represents the core, while the yellow colored exterior sphere the homogeneous surface layer) measured with an arbitrary experimental setup. As it can be seen from the illustration, only the top hemisphere of an unshaded particle is considered for the analysis. This assumption is based on geometrical considerations regarding the positions of the experimental components in respect to each other and to the sample itself. In this context, a hemisphere represents the maximum theoretical probed area when the elements of the setup coincide. Complied with these conditions, it can be noticed that the residual surface layer (colored in orange) after ion etching that will be measured, from the analyzed area (dark orange shaded region), depends on the position of the ion gun in the three dimensional space.

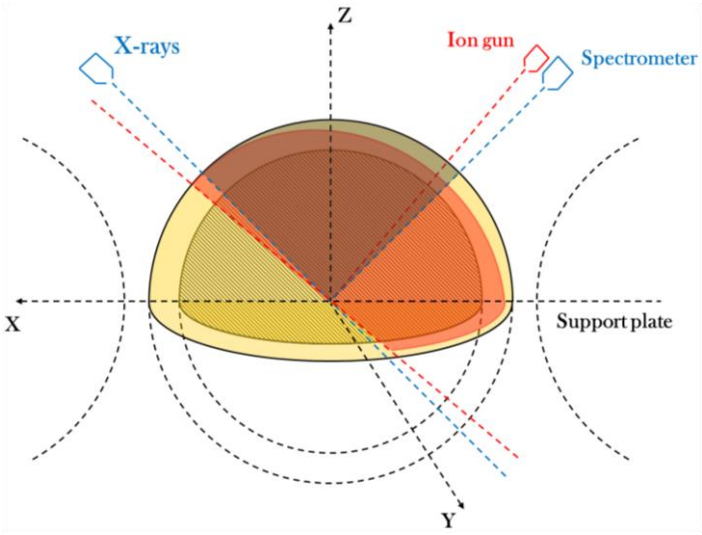

Figure 7: A schematic illustration of the effect of the incident ion beam angle on the analysis of a spherical surface with XPS.

Hence, the purpose of the development of the theoretical model in Paper I was to introduce geometrical freedom in terms of experimental setup and to create a versatile tool that could match the specifications of any equipment used for such type of analyses. In order to do so, each analyzed particle is considered of having a homogeneous surface layer that can extend above the $3\lambda^{ox}$ limit, where λ^{ox} is the attenuation length of the material under investigation, due to the implementation of ion etching for its evaluation. Additionally, as shown elsewhere, an underestimation in thickness determination can occur when analyzing inhomogeneous films [43]. Moreover, the ion gun, the X-ray source and the spectrometer axes are all defined in space by different sets of spherical coordinates for the purposes of the model.

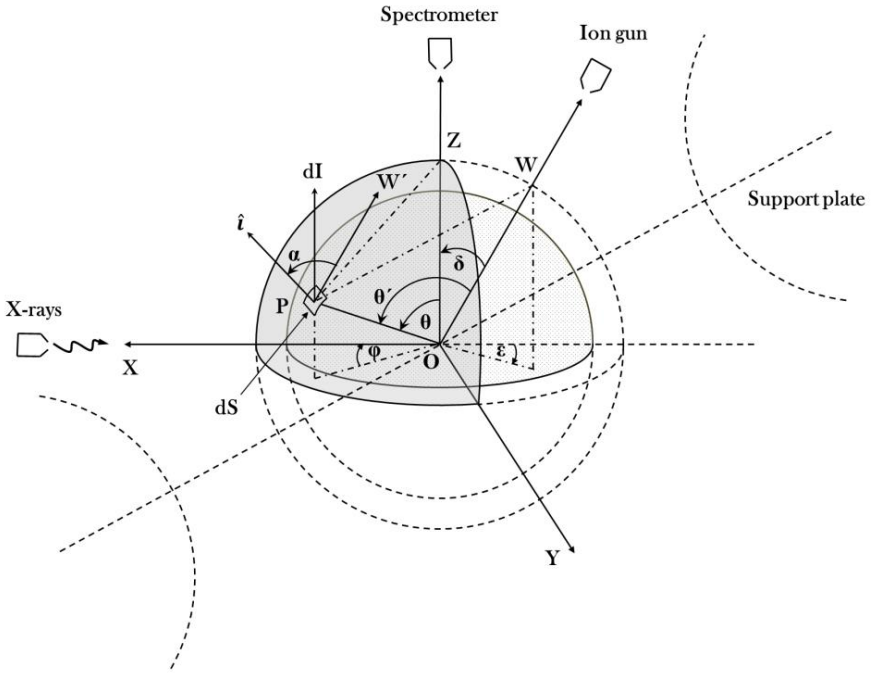

Figure 8: A schematic representation of a spherical core-shell structure analyzed by an arbitrary experimental arrangement in XPS (Image taken from Paper I).

In Figure 8, the spherical coordinates of a random point **P** on the analyzed area of a particle surface (shaded area) are depicted as well as the relationships between the X-ray source, the spectrometer and the ion gun. All these considerations where taken into account and described in Paper I, where a relationship that defines the recorded intensity at each point of interest was formulated according to equation (2):

$$I = iR^2 \int_{\theta_1}^{\theta_2} \int_{\varphi_1}^{\varphi_2} F\, cos\theta\, sin\theta |\cos(\zeta - \theta)| cos\varphi\, d\theta d\varphi \quad (2)$$

The latter, along with an experimentally acquired profile of the sputtering rate in respect to the angle of ion incidence [44], were implemented in order to calculate the residual surface layer (t^{ox}) at every point **P** of the analyzed area. These calculations were carried out utilizing an iterative process with a custom developed computer software for which only the experimental and material dependent parameters mentioned above are needed (Figure 9).

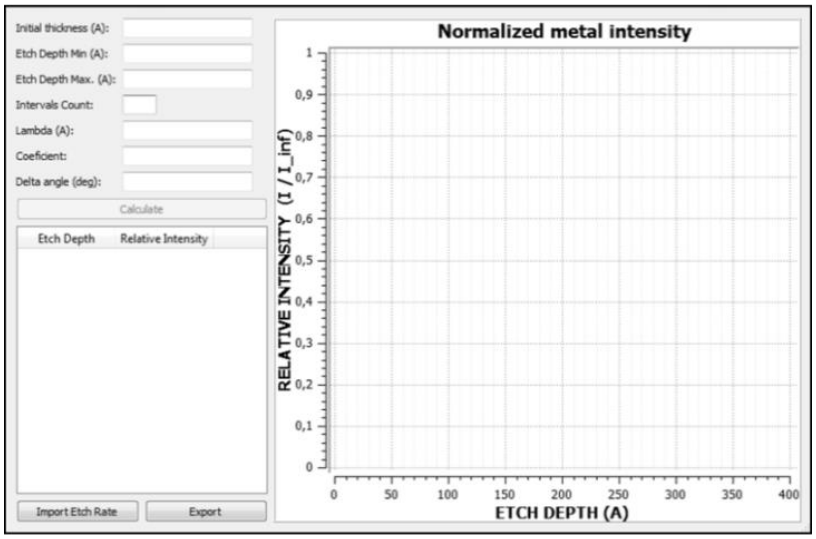

Figure 9: User interface of a developed computer software for calculating the relative substrate intensity *versus* etch depth.

In this manner, characteristic ´*s*´ type curves of the relative intensity of the substrate with respect to the etch depth are acquired for surface layers of known thicknesses and attenuation lengths (λ^{ox}), as shown in Figure 10 for two different materials. These results show that there is a strong dependency of the relative intensity value with increasing λ^{ox} and with increasing layer thickness, where in the first case it increases while in the second one it decreases.

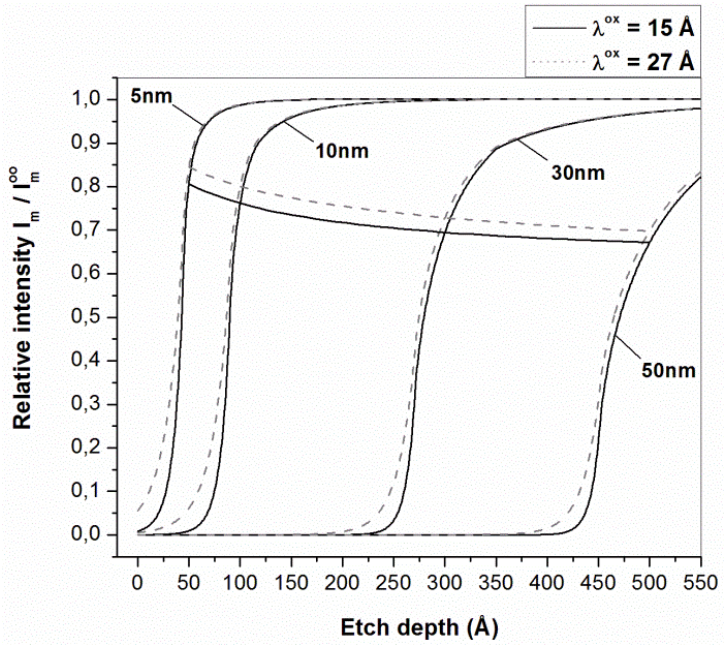

Figure 10: Relative substrate intensities *versus* etch depth calculated for two different λ^{ox} values and different thicknesses of surface layers (Image taken from Paper I).

The theoretical model was experimentally tested on pure iron powder of irregular and spherical shapes, as mentioned earlier in the experimental section, in order to evaluate the effect of the

surface morphology and roughness on the thickness estimation. In addition to the XPS analysis, both grades where cross sectioned with FIB technique and subsequently analyzed with HR SEM in order to determine the thickness variation and homogeneity of the surface layer as shown in Figure 11.

The layer thickness assessment was performed by means of correlating the results from the XPS depth profile measurements from each grade and their respective FIB – HR SEM analyses. The relative metallic intensity values of the experimental XPS depth profiles were acquired for the interface regions, determined by the microscopy analysis, c.f. Figure 11. These values were then correlated with the ones estimated from the theoretical model. This comparison showed a minor deviation, approximately 3%, for both grades that could be attributed to the surface microtopography which introduces a certain degree of localized shading effects, as well as small variation in the layer thickness estimation with HR SEM related to the direction of the FIB cross section (i.e. not accurately performed along the normal of the surface due to the localized topography).

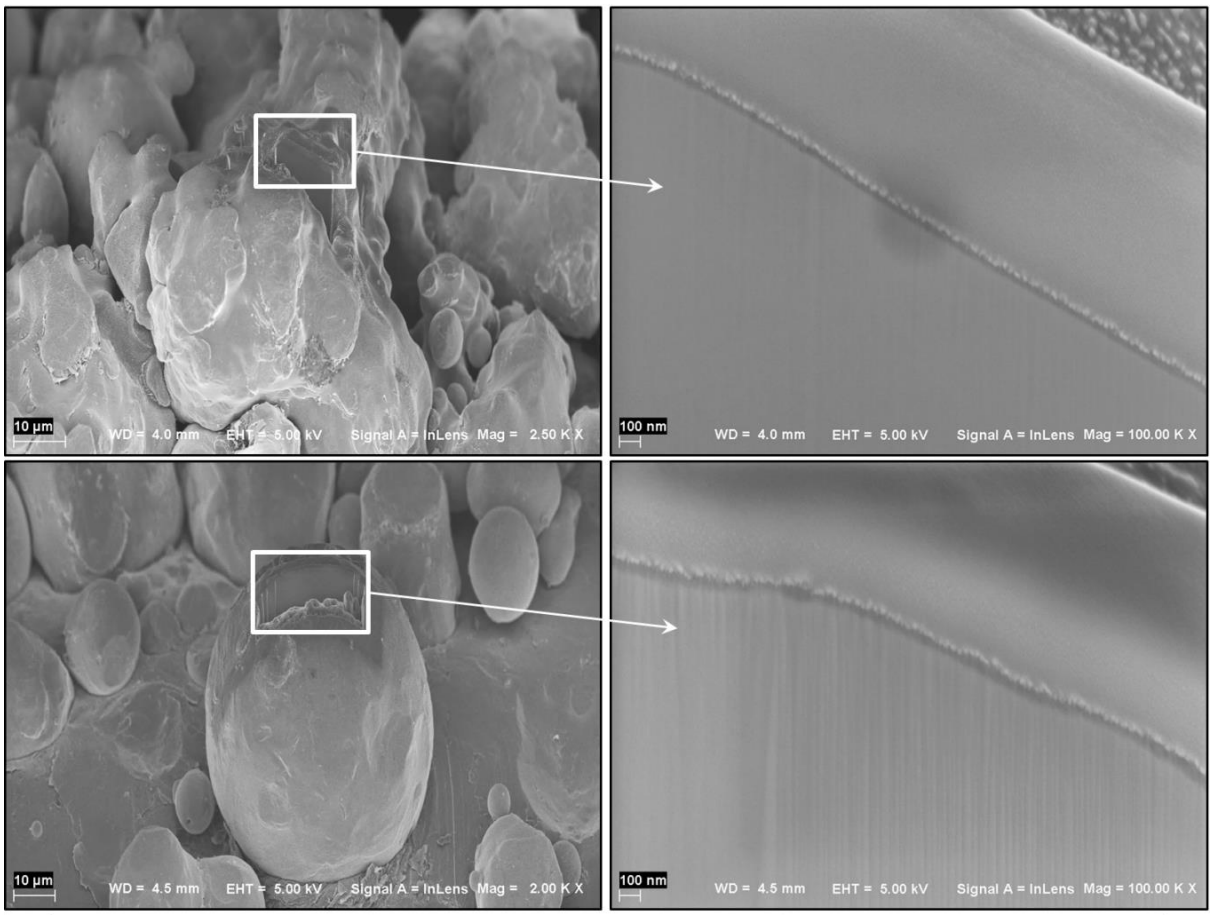

	Water atomized powder	Gas atomized powder
Oxide thickness estimation (FIB - HR SEM)	65.5 ± 14.9 nm	38.14 ± 7 nm

Figure 11: Analyzed cross sections of powder particles from both grades with FIB – HR SEM.

5.2.Investigations on SMC Powder and Processed Components

5.2.1. Surface Characterization of SMC Powder

To characterize the initial state/composition of the insulating coating of the SMC material, a robust methodology needed to be established based on analytical techniques. Initially, the as-received SMC powder was investigated with HR SEM and EDX with different experimental settings in order to determine the optimum conditions for evaluating the coatings morphology, cohesion and coverage of the surface. A range of acceleration voltages from 5 to 20 kV and aperture sizes of 30µm or less were tested in Paper II as to efficiently minimize the beam spot size and interaction volume. The results are shown in Figure 12 where it can be observed that with increasing acceleration voltage, due to the higher energy of the secondary electrons emitted, the information acquired from the very top surface is significantly less and the features of the coating are no longer visible.

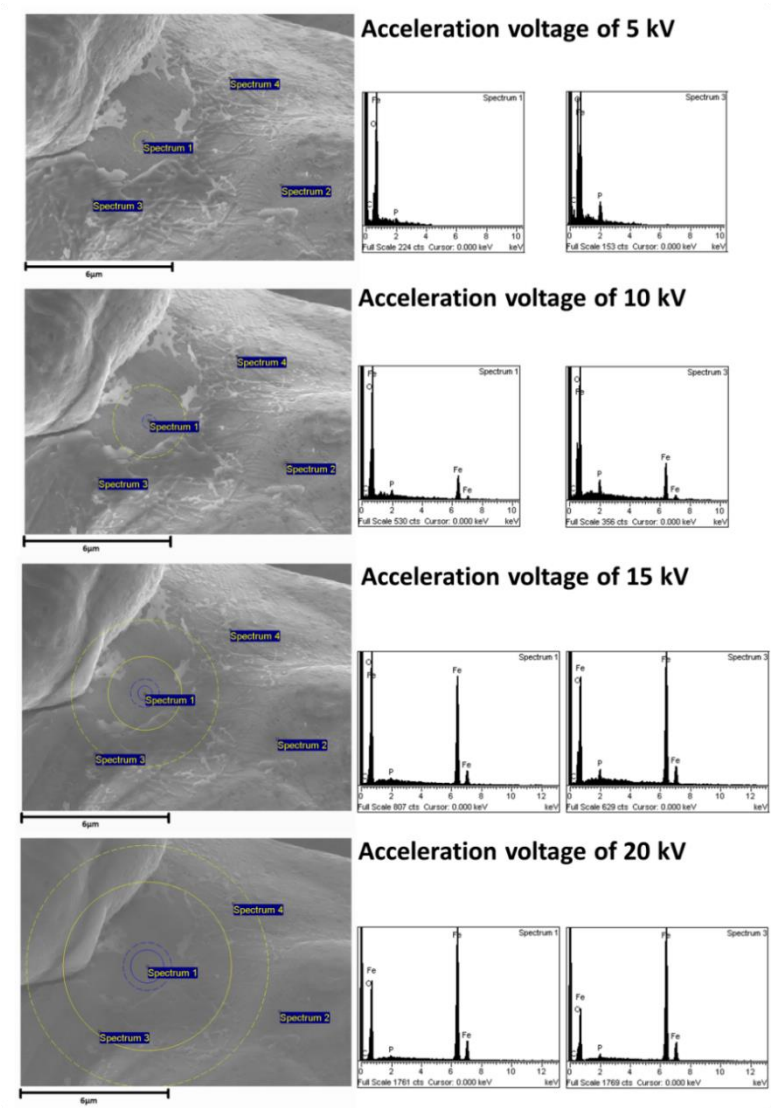

Figure 12: Qualitative EDX point analysis of as-received SMC power under different acceleration voltages (5, 10, 15 and 20 kV) (Image taken from Paper II).

Additionally, regarding the chemical microanalysis, it is shown that at lower acceleration voltage it is possible to still excite all the elements present at the surface layer and better distinguish between the core material and the coating regions. By implementing the above optimum conditions, HR SEM and EDX analysis revealed the good coverage of the particles surface by the insulating layer, its homogeneity in terms of surface feature characteristics and the rare presence of delaminated regions close to the particle irregularities.

For the XPS analysis of the as-received powder, two sample preparation methods were tested as to determine the most suitable one for tackling charging effect during measurements and for ensuring the integrity of the coating. In one case, the SMC powder grade was softly pressed into aluminum plates, while in the other it was loosely spread over adhesive conductive carbon tape. For both methods charge compensation using an electron flood gun and software correction based on carbon C1s signal were implemented. The results revealed the presence of the same elements in the surface for both cases (oxygen, phosphorus, iron, carbon and traces of nitrogen), with the exception of a slightly higher carbon signal for the powder mounted on the carbon tape. It was thus preferred to apply the latter method as the preservation of the insulating coating state was much more ensured, since no mechanical force was applied on the particles during specimen preparation. The chemical compositional analysis of the powder with the HR scans showed that the surface layer consists of ferric and ferrous iron phosphate compounds. The stability of the phosphorus signal to the sputtering operations indicated its homogeneous nature throughout coating thickness depth. Moreover, the analysis of the oxygen signal after successive ion sputtering steps exposed a transition from the PO_4^{3-} group to the O^{2-} compound, which was accounted to the Fe-oxide close to the interface between the matrix and the surface layer. The implementation of the model for layer thickness determination on the as-received SMC powder was also performed based on the XPS depth profiling analysis. The thickness evaluation of the surface layer was estimated based on the normalized signals of its constituent elements (Figure 13). From the latter it became apparent that the coating was in the nano-meter scale and based on the phosphorus signal, which can be solely assigned to the presence of the insulating coating, its thickness could be estimated at about 23 nm.

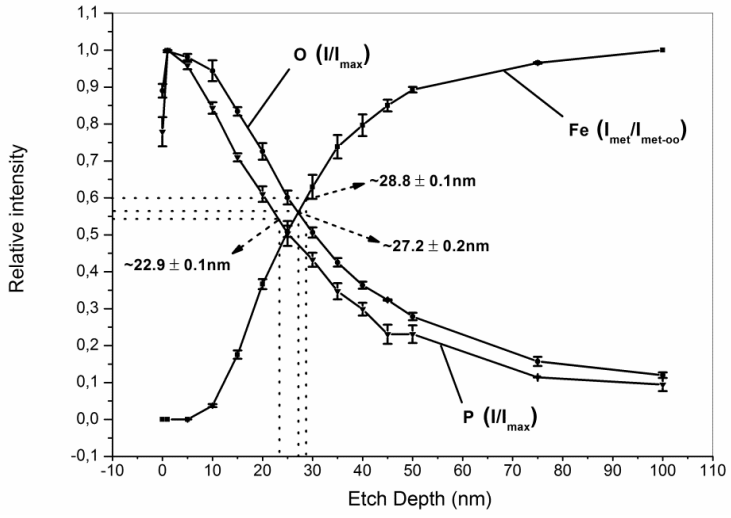

Figure 13: Normalized intensities of Fe metal, oxygen, and phosphorous *versus* etch depth for SCM as-received powder (Image taken from Paper II).

5.2.2. Thermal Stability of the Insulating Surface Layer of SMC Powder

In Paper VI the thermal stability of the insulating surface layer of the SMC powder was investigated. The composite material was analyzed in its as received state, as well as after annealing in oxidizing (air) and inert (N_2) atmospheric conditions. For the purposes of this study, the previously established methodology based on combining HR SEM, EDX and XPS was implemented. The chemical analysis presented in Paper II of the surface nano-layer indicated that it consists of a mixture of iron phosphate compounds and oxides. Due to its thin size though, structural analysis with XRD and thermal analysis with TGA and DSC were not able to yield any information on its crystalline state and thermal stability, respectively. Instead, a parallel investigation utilizing the latter techniques was conducted for chemical standards whose composition could resemble the one present in the surface layer of the SMC material. In more detail, based on the possible mechanisms of coating formation through phosphate conversion treatments [28, 45], iron (III) phosphate dihydrate ($FePO_4 \cdot 2H_2O$) was acquired as a candidate compound and processed under similar conditions as the SMC powder. The crystal structure of the phosphate appears to be XRD amorphous in its as-received, dehydrated and annealed states up to 500°C, where the first minor unidentified reflections start to appear (Figure 14). At temperatures close to 600°C, for both atmospheres, the compound assumes a crystalline structure belonging to trigonal α-$FePO_4$ phase.

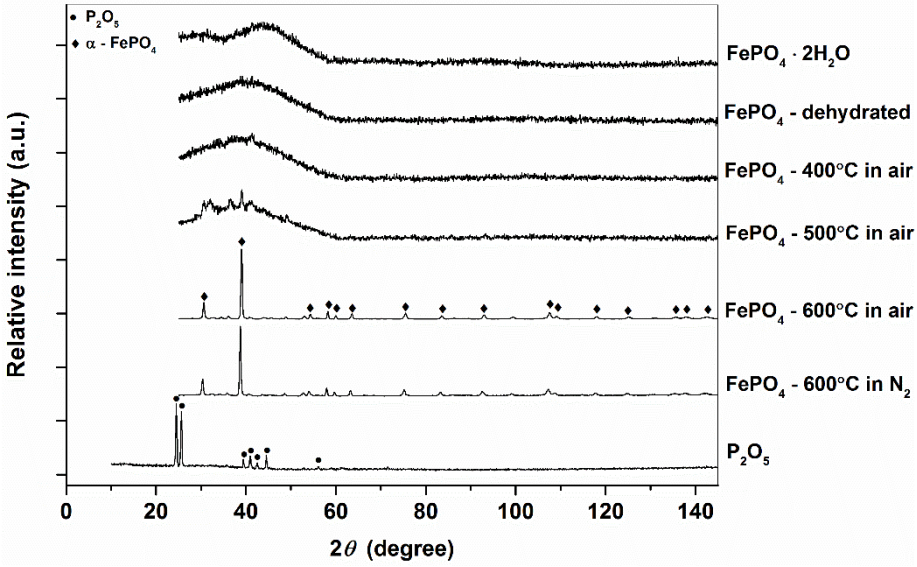

Figure 14: XRD analysis of chemical standards

These results were well correlated with the ones acquired from the thermal analysis measurements with DSC of the same material. There, the two irreversible exothermic peaks observed at 589.9°C and 605.5°C were further correlated with the structural transformation of the iron phosphate (Figure 15). Another interesting feature in this analysis was the presence of an endothermic peak at 550.4°C, indicating a possible glass transition region which is in accordance to what has been reported previously for such compounds [46].

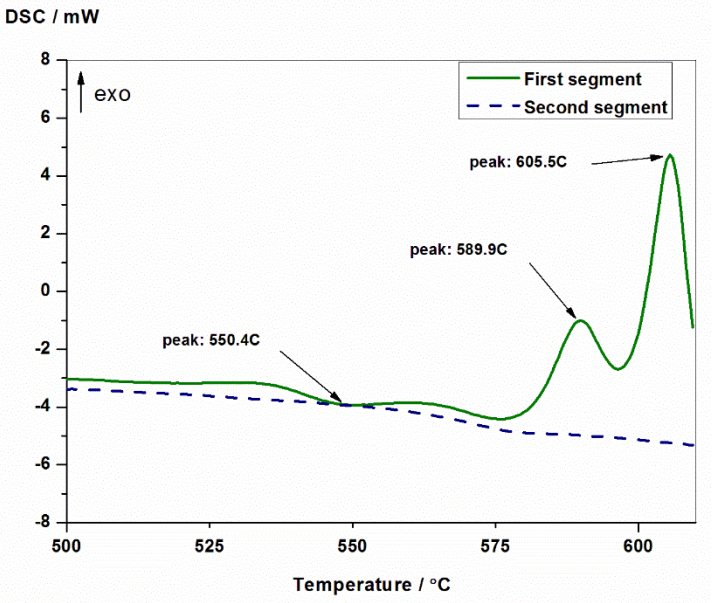

Figure 15: DSC analysis of $FePO_4$ dehydrated in air – heating stage

In addition to the structural and thermal analysis investigations, iron phosphate and phosphorus oxides standards were also analyzed with XPS in order to evaluate their chemical composition and state. The aim of this effort was to determine the stability of such compounds and subsequently utilize this information as reference for the analysis of the SMC powder in all conditions. The peak position values for all elements where acquired by curve fitting opperations, as described in the experimental details section, with few examples on how these envelopes were resolved into their respective components as shown in Figure 16.

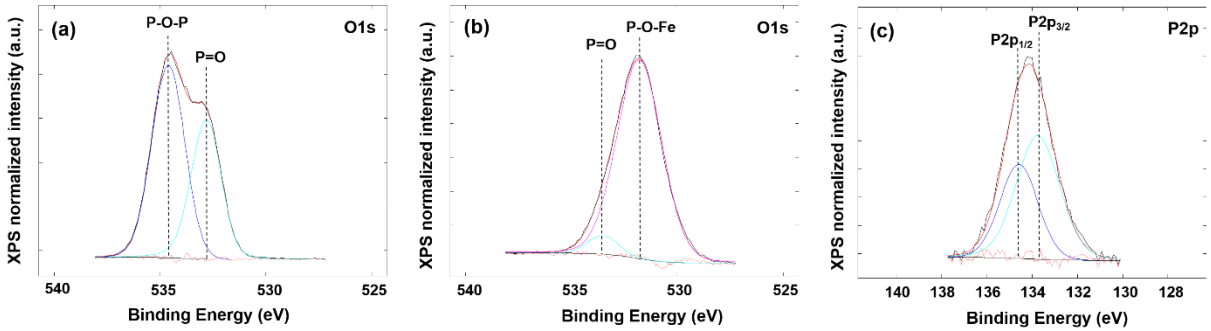

Figure 16: Curve fitting operations for chemical standards (a) P_2O_5 and (b), (c) for $FePO_4 \cdot 2H_2O$

For the case of oxygen signal, a distinction between the different types of bonding in the compounds under question was performed, isolating the contribution from bridging oxygen (P-O-P) and non-bridging oxygen (P=O, P-O-Fe) bonding [47]. Additionally, for the case of phosphorus signal the spin splitting effect was adressed by the fitting process. The results of the XPS analysis for both chemical standards and SMC powder, for all conditions, are summarized in Table 2.

Table 2: List of binding energies of all elements from all high resolution XPS spectra.

Sample	Binding Energy (eV)				
	$Fe2p_{1/2}$	**$Fe2p_{3/2}$**	**$P2p_{1/2}$ / $P2p_{3/2}$**	**O1s**	
$FePO_4 \cdot 2H_2O$	726.2	712.7	134.6 / 133.7	**(P=O / P-O-Fe)**	533.5 / 531.7
$FePO_4$ dehydrated	725.7	712.6	134.6 / 133.7	**(P=O / P-O-Fe)**	533.4 / 531.6
$FePO_4 \cdot 2H_2O$ (600°C in air)	726.1	712.3	134.7 / 133.8	**(P=O / P-O-Fe)**	533.4 / 531.6
$FePO_4 \cdot 2H_2O$ (600°C in N_2)	725.8	712.2	134.7 / 133.8	**(P=O / P-O-Fe)**	533.4 / 531.6
P_2O_5	-	-	136.6 / 135.8	**(P-O-P / P=O)**	534.6 / 532.8
SMC – as received	726.1	712.5	134.7 / 133.7	**(P=O / P-O-Fe)**	533.4 / 531.6
SMC (600°C in N_2)	724.6	711.2	134.7 / 133.8	**(P=O / P-O-Fe)**	533.4 / 531.6
SMC (600°C in air)	724.2	710.8	-	**(OH^- / O^{-2})**	531.3 / 529.8

From such chemical analysis it was concluded that the iron phosphate compound appears to be chemically stable under the thermal treatment employed, since no distinct change from its initial chemical state was denoted. Furthermore, the comparison between the SMC powder and the chemical standards pointed out that the composition of the surface layer of the composite powder in its as received state resembles the one of iron phosphate. After the thermal treatment though a difference was observed in the state of the SMC coating, as shown by the iron and oxygen XPS signals. The presence of iron oxide scale was observed at the top surface after the annealing performed in oxygen, denoting a diffusion mechanism of iron and oxygen through the layer. In nitrogen atmosphere conditions though such an oxide layer was not present, but rather a change in the chemical state of the phosphate compounds in the surface layer was indicated by a shift in the iron XPS signal. These results, as opposed to the ones acquired from the chemical standard analysis, were attributed to the interface interactions between the iron phosphate compounds existing at the surface layer and the readily supply of the available iron from the powder material matrix.

The findings of the structural, thermal and chemical analysis were also correlated to the microscopic investigations of the SMC powder, in as received and processed states. As shown in Figure 17, the nature of the insulating coating alters with the heat treatment in N_2 from an initial "patchy" surface morphology to a more homogenized one with the distinct presence of boundaries. The latter could be attributed to the crystallization or coalescence process of the surface layer from its original form, as also indicated based on the XRD and thermal analysis results.

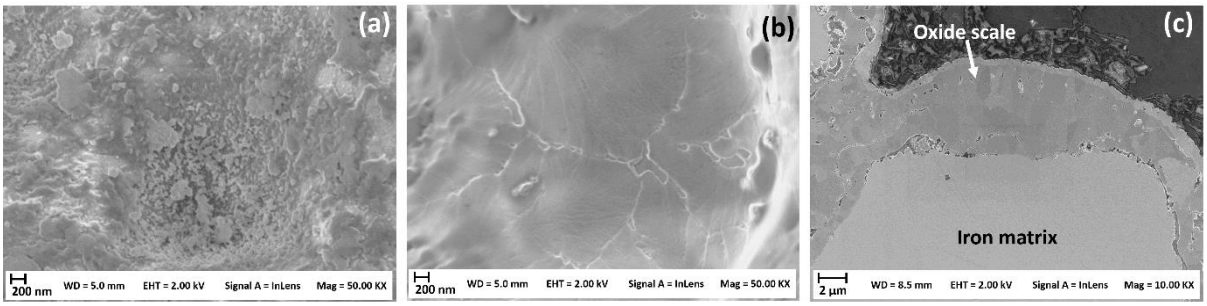

Figure 17: HR SEM analysis of SMC powder: a) as-received state, b) annealed at 600°C in N_2 and c) annealed at 600°C in air (cross section of a powder particle)

Moreover, it was observed and verified by EDX analysis that after the heat treatment in N_2 the coverage of the coating changes, since exposed areas of the powder surface start to appear most probably due to density changes during the crystallization transformation. The formation of a thick oxide scale up to 7 μm in thickness was denoted when annealing the SMC powder in air, as shown by the cross sectional imaging of polished powder particles, while no phosphorus signal was detected with EDX technique. It was concluded thus that under such conditions degradation of the coating occurs.

5.2.3. Surface characterization of SMC processed components

Three different temperatures, namely at 400°C, 500°C and 600°C, where chosen in Paper III in order to investigate the effect of annealing on SMC components. The selection was done based on previous investigations on the magnetic and mechanical properties of such type of materials, where at 600°C it appears to exist an upper limit to their performance [9]. Initial optical stereoscopic micrographs of the fracture surfaces revealed an evident discoloration throughout the cross section of the sample treated at 400°C as compared to the rest, denoting the difference in the effect of the post heat-treatment step between different temperatures. Subsequent HR SEM analyses of both outer and interior regions of the fractured surfaces of all heat-treated components showed a difference in the morphology, homogeneity, coverage and cohesion of the developed surface layer between the different conditions. In the outer regions of all samples a multi-layered thick scale was observed, forming a network between the metal particles as shown in Figure 18.

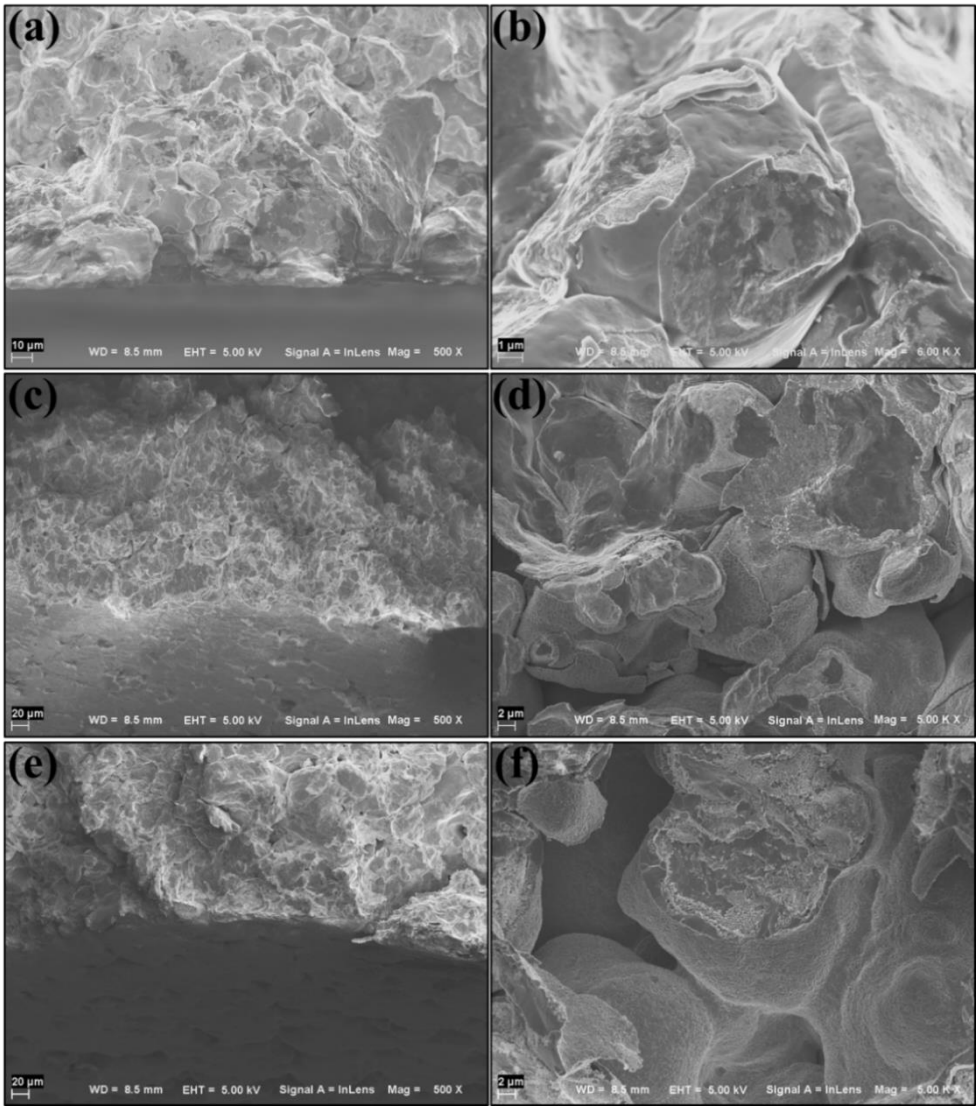

Figure 18: HR SEM micrographs of the outer regions of the SMC heat-treated components at 400°C (a-b), 500°C (c-d) and 600°C (e-f).

The analysis of the surface of the exterior region of the SMC components with XRD under grazing angle showed that the scale consisted of iron oxides, mainly magnetite and hematite. It was also noted that its thickness was increased with the annealing temperature. These results were also in accordance with the qualitative point analysis performed with EDX technique on the scale for all temperatures, showing that iron and oxygen were the main constituent elements. Contrarily, the surface layer present in the interior region of the parts appeared to be very thin as compared to the outer region, while additionally two morphologically distinct areas were observed in it. These were easier to differentiate at higher magnifications, as shown in Figure 19 (b, d and f), where the open areas inside the parts exhibited clean powder surface, while at the areas at which particles are connected there was a 'net' type of structure with different imaging contrast present. In particular, after treatment at 400°C, the latter areas are more pronounced and their EDX chemical microanalysis showed an enrichment in carbon and zinc as compared to the matrix material. These results indicated the presence of residual chemical compounds, supposed to be directly related to the incomplete de-lubrication of the parts at those temperature regimes.

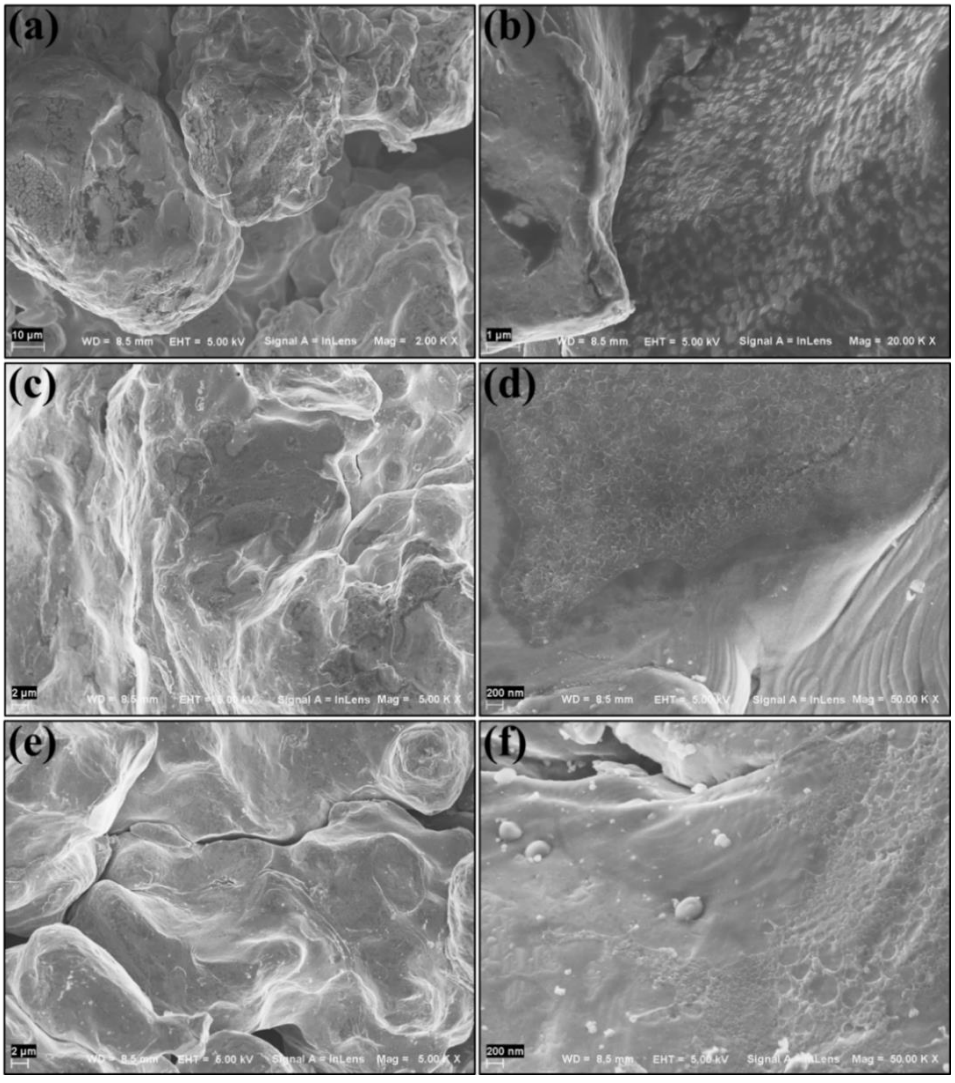

Figure 19: HR SEM micrographs of the interior regions of the SMC heat-treated components at 400°C (a-b), 500°C (c-d) and 600°C (e-f).

To further investigate the effect of the annealing temperature on the surface coating, XPS analyses were performed for both the interior and exterior regions of all samples. The apparent atomic concentrations showed that for the outer regions a higher amount of carbon is always detectable as compared to the interior, implying that the residuals of the organic-based lubricant containing heavy hydrocarbons are decomposing in the outermost surface of the component. Moreover, the carbon content on the fracture surface of the interior region of the sample treated at 400°C was also higher as compared to the samples treated at higher temperatures, showing that the incomplete de-lubrication is even more evident for the lowest temperature among the ones tested. Additionally, the XPS analysis for all surface layers, for both regions, indicated that the layers consist mainly of a mixture of iron oxides and iron phosphates of both divalent and trivalent forms. In particular, the oxygen signal after analysis at 400°C showed that the oxidation was more pronounced in both regions compared to that of the other samples. By coupling these results with the ones from HR SEM imaging and XRD analysis it was concluded that the insufficient closure of the external porosity from the oxide scale growth at low temperatures lead to the extended oxidation of the component throughout its cross section. By further analyzing the HR XPS spectra, the ratio between the phosphorus and iron content was evaluated for the interior regions of the annealed SMC components investigated in Paper III, as well as the as-received powder studied in Paper II (Figure 20). A significant drop of the ratio was observed in depth for the components as compared to the loose powder, with the sample heat-treated at 500°C having the highest measured value followed by the ones treated at 600°C and 400°C, respectively. Such analysis can be considered as a qualitative measure of the effect of annealing to the chemistry and thickness of the coating and can be linked to the degree of oxidation for each treatment condition, as mentioned previously.

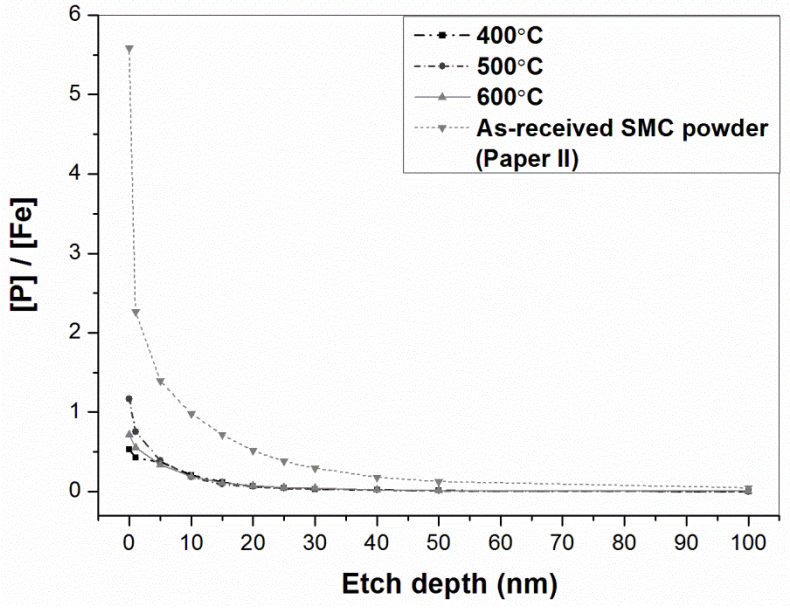

Figure 20: Ratio of phosphorus and iron content *versus* etch depth for all heat-treated samples from Paper II (interior regions) and as-received powder from Paper III.

In addition to the aforementioned results on the surface chemistry of the surface layer of the heat-treated SMC components, the presence of a small secondary peak was observed after ion sputtering for all conditions in the phosphorus signal. Its presence was not attributed to the PO_4^{3-} species but to transitional metal phosphides. Theoretical thermodynamic calculations performed in Paper III supported their existence close to the interfacial region between the surface layer and the matrix due to the abundance of iron and the low oxygen partial pressure that exist in a PM compact.

Finally, the theoretical model was qualitatively implemented to the fracture surfaces under the considerations that the degree of surface roughness was acceptable and reproducible based on the small standard deviation values from the repeated measurements (Figure 21Figure 21). By doing so, the relative intensities of iron signal showed that the total surface layer at 400°C was the thickest observed for all conditions. For the other two temperature regimes, at 500°C and 600°C, the differences were too small and comparable to the standard deviation. The relative intensities of the phosphorus signal though showed that all temperature profiles are very close to each other, with the one at 400°C being the broadest followed by the 500°C and 600°C. By combining all this information from these profiles and the one from the P/Fe concentration ratio analysis depicted in Figure 20 it may be plausible to assume that at 400°C the open porosity of the sample allows further oxidation in its interior region and thus the presence of a thicker oxide layer. For the cases of 500°C and 600°C though the growth of the exterior scale prevents this mechanism to take place to a great extent. Still though, oxygen diffusion through the scale takes place in both of these cases and in particular at 600°C, where the kinetics are faster. A slight increase in the thickness of the surface layer is observed as compared to the one at 500°C due to its further oxidation. The latter can also correlate to the HR XPS spectra analysis of the oxygen signal, where the O^{2-} shoulder is slightly broader for the fractured sample heated treated at 600°C.

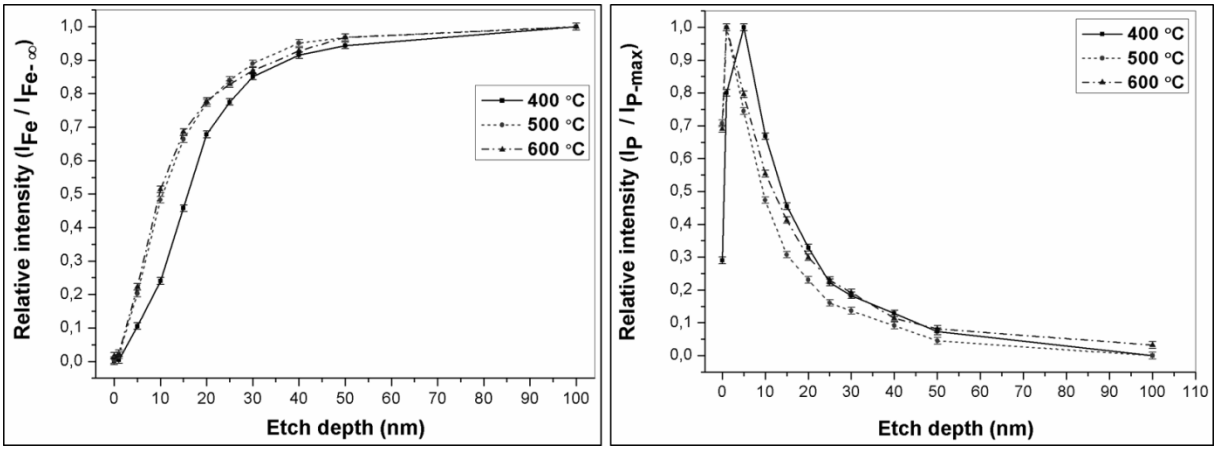

Figure 21: Normalized intensities of interior regions of SMC components heat treated at 400, 500 and 600 ˚C for Fe metallic (left) and phosphorus (right) signals vs etch depth. (Image taken from Paper III)

5.2.4. Microstructural development and deformation state of processed components

In Paper IV the compressive behavior of high purity and pre-alloyed iron powder was modeled and experimentally investigated. A comparison was made between the two grades in order to determine and evaluate those factors that influence their compaction to a green body and at which extent. Initially, a semi-empirical model was implemented as to quantitatively assess the compaction process of the grades, based on the progression of two numerical parameters that take into account the geometrical characteristics of the powder particles and their ability to plastically deform. The relationship that describes and relates the aforementioned parameters to the porosity of the compact part at a certain applied pressure can be written as follows:

$$P = P_0 \exp(-Kp^n) \qquad (3)$$

In equation (3) P is the porosity at the applied pressure p, P_0 is the porosity at zero pressure (i.e. experimentally measured apparent density), K is a parameter that accounts for the geometrical characteristics of the metal particles and n is related to the ability of the particles to plastically deform (ranging between values of 0.5 and 1; the higher is the value the lower is the ability of the particle to plastically deform). To experimentally implement the compressibility model, compressibility curves and apparent density measurements were acquired from four sieved fractions from each powder. The latter division of the grades based on particle size was performed in order to additionally link the particle size distribution to the findings of the study. Based on the results, the high purity iron powder exhibited the least effect of particles geometry and morphology to its compaction along with the highest capacity for plastic deformation for all sieved fractions. The findings also indicated important differences at the intermediate particle size fraction between the two grades, which lead to the conclusion that the compressibility behavior of the pre-alloyed powder could be improved by optimizing further its particle size distribution. Further correlation of the results of the compressibility model to ejection energy measurements indicated that the compaction process is taking place in two stages. In the first stage, at pressures below 400 MPa, particle rearrangement is the major contributing factor to densification, whereas in the second stage at higher pressures plastic deformation is the dominant mechanism.

In order to further investigate the predicted compaction behavior by the model for the grades in terms of their capacity for plastic deformation, an internal microstructural evaluation of the powder particles was performed. In Paper IV a methodology based on EBSD and EDX techniques was developed for investigating the cross sections of loose powder particles. For EBSD "imaging" a scalar value was utilized that is mapped in grayscale and measures the quality of the processed diffraction patterns, known as band contrast (BC) [38]. Such information was overlaid with elemental mapping from chemical microanalysis with EDX as shown in Figure 22. In addition, the crystallographic orientation obtained from all analyzed grains was presented with an Euler angle-based color scale (red, green and blue for Euler angles φ_1, Φ and φ_2 respectively) and combined with EBSD "imaging". From such analysis, it was

shown that for the high purity iron powder, a distribution of grains with sizes varying from few micrometers to few tenths of micrometers is present, having randomized crystallographic texture. Moreover, the existence of oxide inclusions located at the junctions of grain boundaries was also noticed, indicating an additional strengthening mechanism for the material by hindering the movement of the latter. It was thus shown that such type of microstructural features could be considered responsible for the compaction behavior of the different powders, as described by the semi-empirical model.

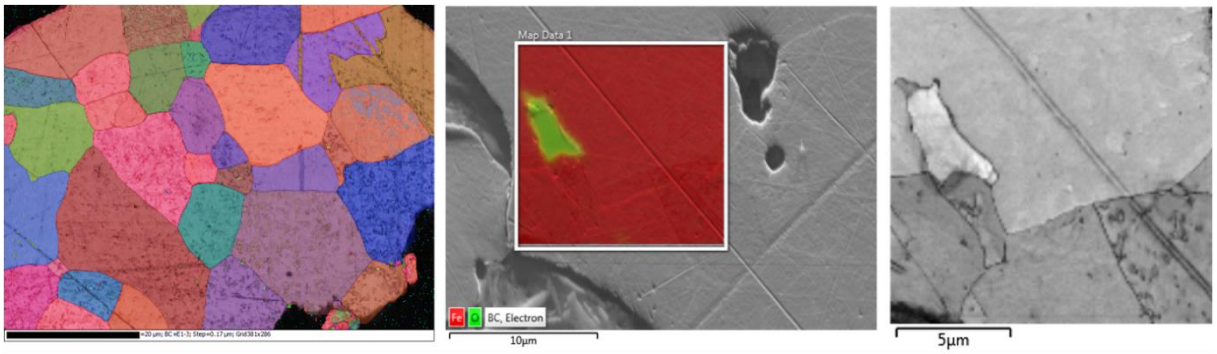

Figure 22: EBSD/Euler angles (left), EDX (middle) and band contrast (right) maps for ASC100.29 un-sieved sample (scale bar on the EBSD map equals to 20 µm)

The methodology followed in Paper IV for the investigation of the internal microstructure of powders was further developed and implemented in Paper V, in order to assess in this context the effect of the compacting and annealing process steps in the SMC components. A further correlation of those findings to their performance was also presented. For such purposes EBSD maps were acquired, analyzed and correlated to nanoindentation and magnetic properties measurements for pressed parts in green state and annealed at 400°C, 500°C, 550°C, 600°C and 650°C.

Initially, the evaluation of the microstructure and state of deformation of the processed SMC components was performed by coupling EBSD maps from single powder particles and nanoindentation measurements from the same regions (Figure 23). With EBSD analysis a distinction between low angle grain boundaries (LAGBs) and high angle grain boundaries (HAGBs) was made, with the former having a misorientation of 2-15 degrees and the latter above 15 degrees. The HAGBs indicated the presence of the grain structure internally in the powder particles and depicted its development with temperature. Additionally, the LAGBs enabled the visualization of the localized residual plastic strain in the material after processing, since the high concentrations of LAGBs are linked to the presence of high density of "geometrically necessary dislocations" (GNDs) due to plastic deformation of the material [37]. The nanoindentation measurements also verified the differences in hardness between the areas where the density of LAGBs was high as compared to areas where the latter were low, providing with quantitative values on the degree of deformation of the material. As shown in Figure 23 the highly strained regions were located mostly at the rim of the powder particles, where particle to particle contacts exist during pressing. The amount of LAGBs was also found to be

diminishing substantially with increasing annealing temperature, pointing out to the relaxation of strain to the material.

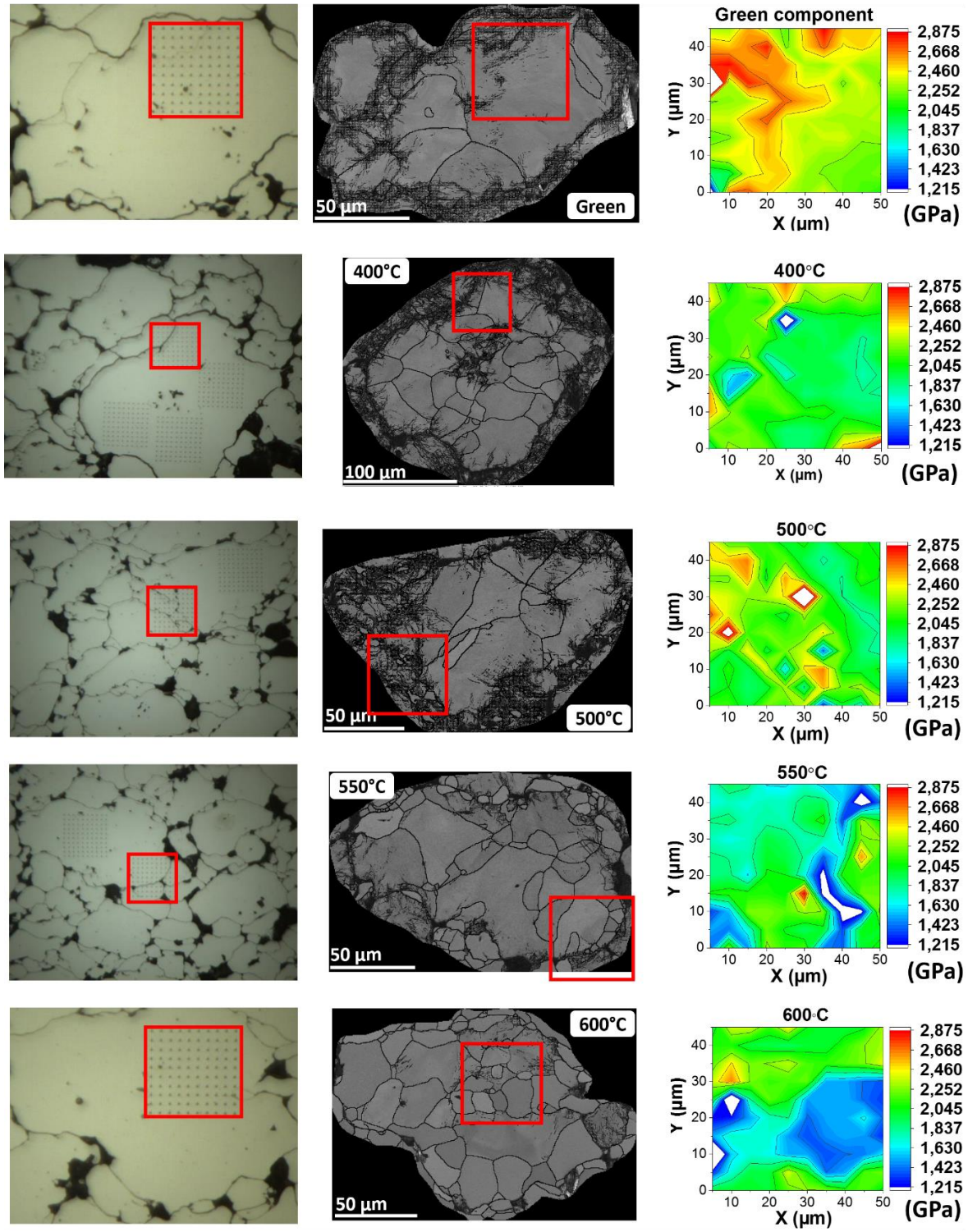

Figure 23: Optical microscope images/nanoindentation arrays (*left column*), EBSD images (thick lines represent HAGBs, thin lines represent LAGBs) (*middle column*), Hardness contour maps (*right column*)

A further correlation of the nanoindentation and EBSD measurements was made in Paper V in order to map the plastic deformation in SMC parts, based on the internal average misorientation angle for each measured grain [37]. For such purpose, the misorientation angle limits in the EBSD analysis that would dictate the deformed, substructured and recrystallization/recovery fractions were set in correlation to the nanohardness values acquired from the different areas in the material. An example is shown in Figure 24 where the newly recrystallized, strain free, grains can be distinguished from the highly deformed ones, in which the density of LAGBs is high, or the substructured ones, i.e. having subgrain structure. Moreover, utilization of the recrystallization/recovery fraction enables quantitative results in assessing the amount of deformation in the material, rather than only visualizing its presence.

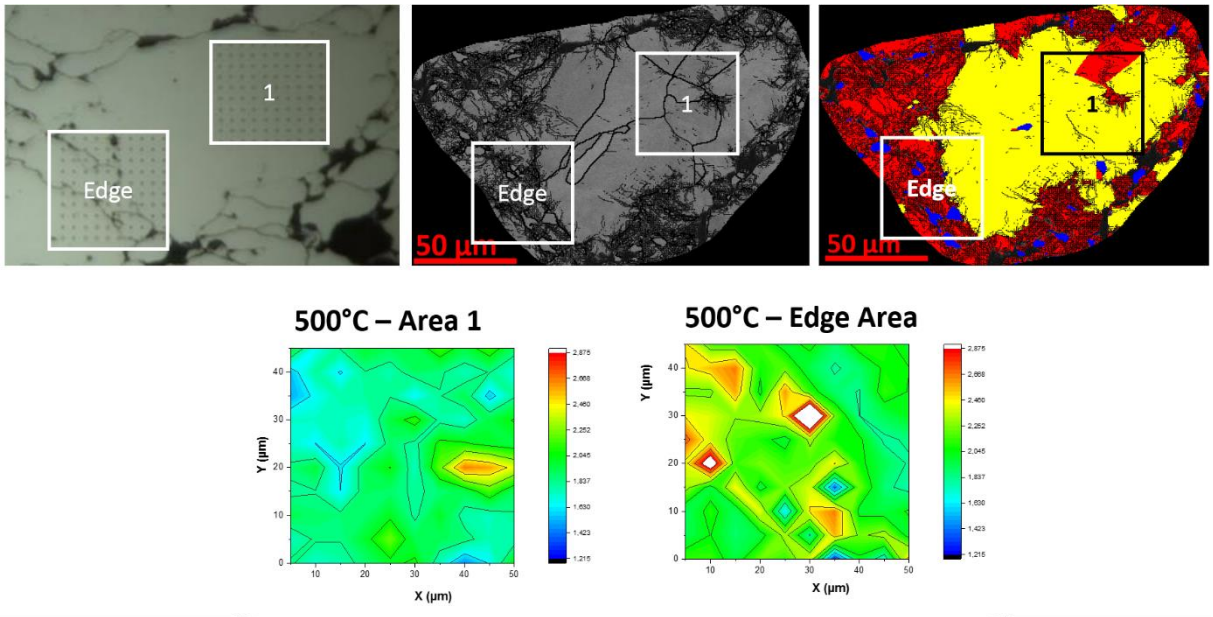

Figure 24: Correlation of nanoindentation measurements to the recrystallization/recovery fraction analysis with EBSD (red color is for the deformed grains, yellow for the substructured grains and blue for the recrystallized/relaxed grains).

Similar EBSD analyses was subsequently implemented in larger areas of the treated samples in order to fully characterize and quantify the development of their microstructure and deformation state. Based on the results from such type of analyses, which can be summarized in Figure 25 and Table 3, information on how the annealing process proceeds in a powdered material and its different stages is obtained. A general reduction in the volume of LAGBs was observed, in combination to a decreasing trend in the area of the grains with increasing temperature. Additionally, an increase of the grain boundary length was denoted up to 500°C followed by a progressive decline at higher temperatures (Figure 25). From these results, it was possible to define the onset of the recovery and recrystallization stages in the SMC parts at the temperature regime of 500-550°C, by a mechanism of growth and coalesce of the newly recrystallized grains emerging from the heavily deformed areas which are located at the edges of the powder particles. Moreover, by utilizing the recrystallization/recovery fraction for these areas the amount of the final relaxation introduced to the components after treatment was

assessed, indicating that for more than 90% of the grains this is achieved at temperatures above 650°C (Table 3).

Finally, a random crystallographic texture was denoted in Paper V for SMC components based on pole figures acquired with EBSD analysis. This texture is retained under all processing conditions and can be considered to contribute to the isotropic behavior of the material.

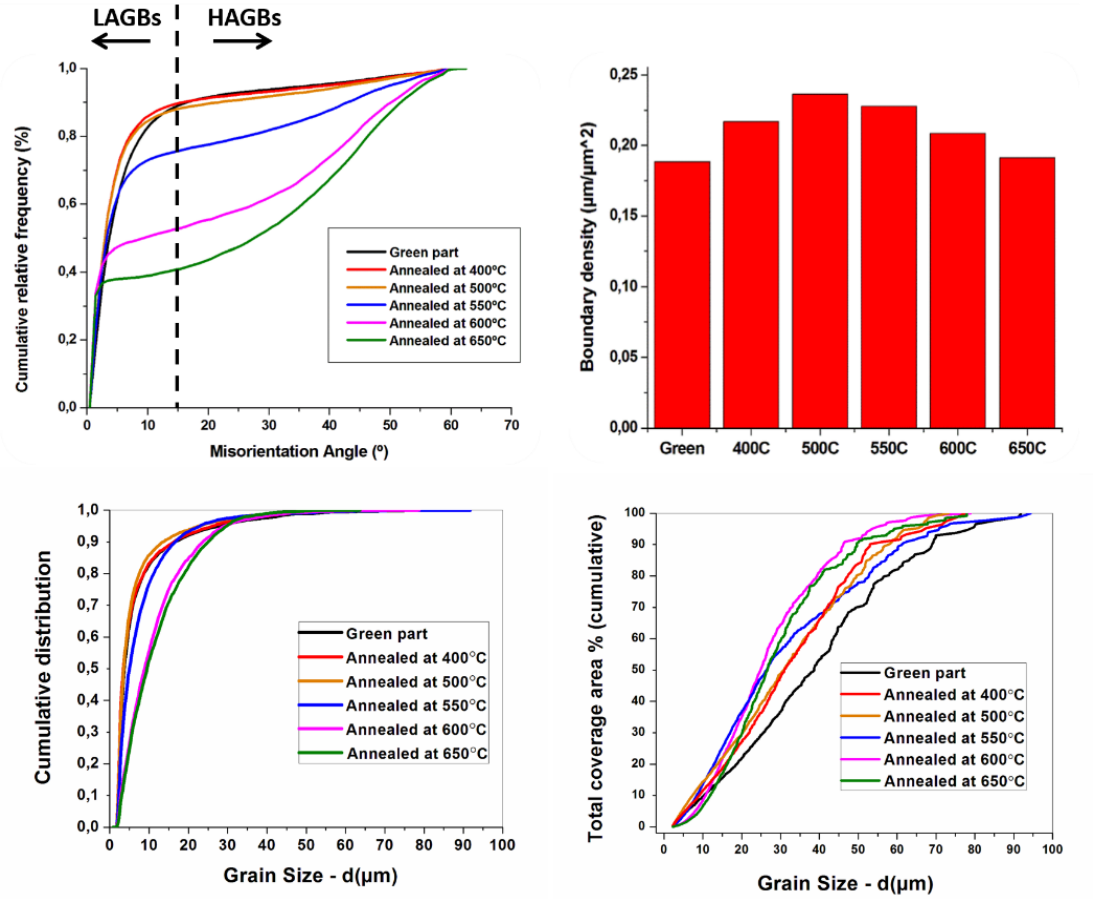

Figure 25: EBSD analysis of SMC treated components. Misorientation angle distribution (top felt), grain boundary density (top right), grain size distribution (bottom left), grain area distribution (bottom right).

Table 3: Mean and median grain size values for all SMC treated components. Recrystallization/relaxation fraction for all SMC treated components.

	Deformed (%)	Substructured (%)	Recrystallized / Recovered (%)	Mean (µm)	Median (µm)
Green part	79.3	20.1	0.6	7.5	4
Annealed at 400°C	69.7	29.5	0.8	7.1	3.7
Annealed at 500°C	80.9	16.5	2.6	6.6	3.9
Annealed at 550°C	56.4	17.8	25.8	8.1	5.4
Annealed at 600°C	3.2	10.3	86.5	11.7	9.3
Annealed at 650°C	0.3	8.7	91	12.2	9.9

5.2.5. Effect of processing on the performance of SMC components

The magnetic properties of the SMC processed components were evaluated based on magnetic tests in both DC and AC conditions. Under DC conditions, as shown in Figure 26, the hysteresis losses and coercivity progressively reduce with increasing temperature, while the permeability of the parts is increasing. Their properties appear to reach a steady state at the temperature regime between 600-650°C where the changes are not so pronounced. At that temperature range, as shown in Papers III and VI, the insulating surface layer of the SMC material is degrading from its initial state. Hence, the improvement on the properties of the material exhibited by the aforementioned measurements is associated to the development of the internal microstructure and deformation state of the processed parts. As shown in Paper IV, the relaxation of most of the residual strain of the material at those temperature regimes, along with the stabilization of the microstructure which is denoted on the grain size and area distributions, are directly linked to their magnetic behavior.

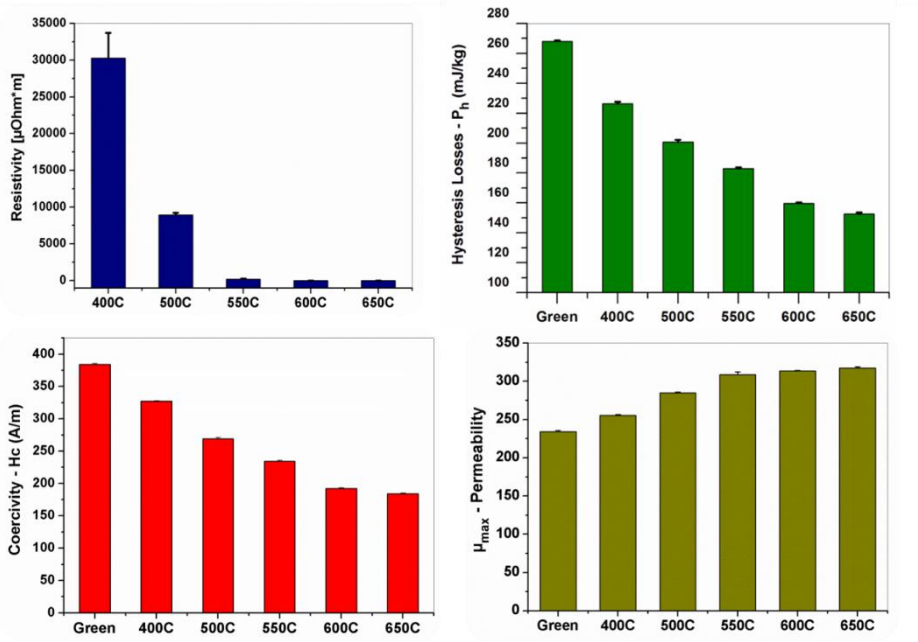

Figure 26: Resistivity (top left), hysteresis losses (top right), coercivity (bottom left) and permeability (bottom right) measurements of SMC treated components.

Finally, magnetic properties tests in AC conditions were also performed for the processed SMC parts for different inductions, an example of which is shown in Figure 27. The linear relationship of the core losses over frequency *vs* frequency indicate their dependency to the eddy current losses developing in the material. By performing linear fitting analysis on such measurements the slope value of the fit can be acquired, which represents the progression of the eddy current losses with frequency. At Table 4 the values of the slope for all conditions at 1T induction are depicted, in addition to the hysteresis losses from the DC measurements. By correlating these findings it becomes obvious that the progressive reduction of the hysteresis losses along with the increase of the eddy current losses at increasing temperatures are both contributing to the total measured core losses. The degree of stress relaxation induced to the material and its

microstructural development with annealing are responsible for bringing the total losses to lower values, while the viability of the coating close to its initial state and structure ensure its stability at higher frequency ranges. Above the critical point of 550°C a sharp increase in the total losses is noted, which can also be related to the decrease in resistivity shown in Figure 26. This behavior is mainly linked to the change in the nature of the surface layer, as shown by the results of the present thesis. In this manner, the contribution of the processing to the performance of the products can be isolated and regarded from a material science point of view for such products.

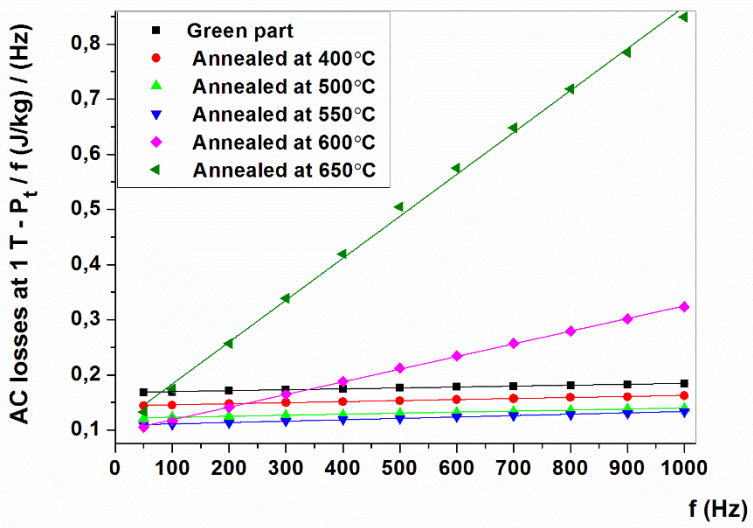

Figure 27: Core losses over frequency *vs* frequency at 1T induction for all SMC processed components.

Table 4: Coefficient values from curve fitting of core losses at 1T induction and hysteresis losses for all SMC processed components.

SMC component	Slope Value	Hysteresis Losses (mJ/Kg)
Green part	1,68E-5	267,92
Annealed at 400°C	1,86E-5	226,32
Annealed at 500°C	1,87E-5	200,64
Annealed at 550°C	2,48E-5	182,97
Annealed at 600°C	2,29E-4	159,67
Annealed at 650°C	7,60E-4	152,66

6. Conclusions

In the present thesis, the following concluding remarks can be highlighted:

Theoretical model for thickness evaluation of surface coatings on metal powder

- A theoretical model has been developed for estimating the thickness of surface layers on particles of spherical shape using XPS depth profiling technique, without any geometrical constraints related to the experimental arrangement. The model was further extended for estimation of the surface layer thickness on the irregular water atomized powder particles.
- The model was experimentally tested with XPS and validated using FIB - HR SEM analytical techniques. The deviation between theoretical and experimental mean values was of the order of 3%.
- It is possible to apply the model with good agreement for routine measurements on surfaces of specific geometry and roughness in the range of up to hundred micrometers.

Methodology development for surface analysis of SMC powder

- A methodology was developed for evaluating the composition, morphology and thickness of the insulating layer of SMC powder grades.
- Optimum conditions for HR SEM and EDX analysis were defined at 5 kV acceleration voltage and low beam current using in-lens secondary electron detector.
- Adhesive carbon tape was evaluated as the optimal method for sample preparation for XPS analysis.
- Surface chemical analysis reveals oxygen, iron, and phosphorous as the main constituents of the insulating coating.
- The surface coating was found to be stable under ion sputtering operations.
- Coating thickness evaluation based on the normalized intensities of the metallic iron, phosphorus and oxygen XPS signals show that it ranges bellow 30 nm.

Thermal stability of phosphate based insulting surface layer for SMC material

- The thermal stability of SMC iron phosphate based surface layer was investigated in both oxidizing (air) and inert (nitrogen) atmospheres by means of XPS.
- References for XPS spectra interpretation were acquired from high purity chemical standards that were processed and analyzed in similar conditions as the composite powder.
- Structural transformation of the pure iron phosphate from amorphous to crystalline was noted in the temperature range between 550°C to 600°C , while no alternation in its chemical state with XPS was observed independently of the processing atmosphere.
- The surface insulating layer of the SMC powder exhibited transformation from its as received state to an oxide scale in air, while in inert conditions the presence of iron phosphate compounds were observed with an altered chemical state.

Surface characterization of heat-treated SMC components

- The effect of temperature on the surface layer morphology, homogeneity, cohesion and composition was evaluated using XPS, HR SEM, EDX and XRD techniques for SMC annealed components.
- For all temperatures two regions, an exterior and an interior, can be distinguished having significant differences in the degree of oxidation.
- For all temperatures the exterior region appears to be considerably oxidized and the presence of an iron oxide scale that increases in thickness with temperature was confirmed as the dominant surface constituent.
- Analysis of all interior regions revealed the presence of a blend of iron phosphates and iron oxides both in divalent and trivalent form.
- The presence of impurity oxide particulates and iron phosphide precipitates dispersed in the insulating surface layer were confirmed as a result of the post heat treatment.
- Analyses based on HR SEM, EDX and XPS techniques depicted the presence of higher amount of lubricant residuals enriched in Zn, due to the incomplete de-lubrication process, for the interior region of the sample treated at 400°C.
- Qualitative implementation of a theoretical model for surface layer thickness determination based on XPS depth profiling showed for 400°C that the insulating layer is associated with a broader profile, i.e. more extended presence along the etch depth, which can be attributed to stronger presence of iron oxides.

Assessment of microstructural development and deformation state of processed SMC components

- A methodology was introduced for investigating the development of internal microstructure and deformation state of powder components based on EBSD, HR SEM, EDX and nanoindentation techniques.
- Correlation between nanoindentation and EBSD results offered visualization and quantification of the degree of deformation after processing for SMC components.
- It was shown that the highly deformed regions in a part are located mainly at the rim of the powder particles, close to the particle to particle contacts. That majority of the plastic strain stored in the material was relaxed at temperatures above 600°C.
- A fine grain structure of few tenths of micrometer was observed in the powder particles of SMC components. The recrystallization stage of the material was assessed based on the evolution of the grain size/area distributions and grain boundary length for the processed parts.
- The SMC components were shown to retain a randomized crystallographic texture in all processing conditions.

Correlation of material properties to the performance of processed SMC components

- A progressive reduction on the hysteresis losses of the SMC treated parts was noted, reaching a more stable condition at the temperature range of 600-650°C. This behavior is correlated to the degree of relaxation of the material at those temperatures, which reaches the amount of 90% according to the EBSD results.
- The eddy current losses of the processed SMC components were observed to sharply increase above 500°C. This results was correlated to the behavior of the insulating coating and its transformation at that temperature regime.

7. Suggestions for future work

7.1. Theoretical model development

For further experimental validation of the theoretical model, point analysis with the Auger electron spectroscopy (AES) along with transmission electron microscopy (TEM) on powder particle cross sections are suggested. These techniques can be utilized in order to fully characterize the materials under investigation and so to eliminate any ambiguities with regard to their thickness evaluation.

Furthermore, the theoretical model is possible to be extended to surfaces of higher roughness, e.g. fracture surfaces, and acquire quantitative results. In order to do so, it must be combined with development of methods or techniques that take into account roughness on a micro-level, allowing thus local point quantitative analysis of non-planar surfaces.

7.2. SMC analysis

Analysis based on a combination of TEM and atom probe tomography (APT) techniques can yield additional information, on atomic scale, on the chemistry and structure of the SMC material at the interface of the insulating coating with the matrix. This information will further provide knowledge on the mechanisms of diffusion of species though the surface layer.

Moreover, additional analysis by AES on the fractured surfaces could reveal more information on the nature of the phosphide phases present as well as information on the composition and thickness of the coating between particle to particle contacts and open (pore surface) areas.

A study focused on the effect of lubricant on the surface chemistry of the SMC material and their delubrication stage is recommended. The techniques and methods utilized in this thesis can provide with the necessary information for further investigating the role of lubricant to the performance of a treated component.

Finally, a detailed thermodynamic study of the Fe-P-O system at different temperatures and processing atmospheres, for the establishment of the phase stability regions and amorphous/crystallographic transformation in the system, is recommended. Kinetic and diffusion studies of the Fe-P-O system is of vital importance for the evaluation of the mass transfer mechanisms in the material through the coating interface. In this manner, the temperature ranges of its stability at specific processing conditions can be determined.

8. Acknowledgments

I would like to thank and express my sincere and deepest gratitude and admiration for both my supervisor Professor Lars Nyborg and co-supervisor Associate Professor Eduard Hryha. My PhD journey has proved to be a great school for me in many ways and both of them have contributed immensely to it with their efforts.

I would like to also acknowledge and thank all my co-authors and colleagues with whom I had the pleasure in collaborating with in my time as a PhD student.

Höganäs AB in Sweden is acknowledged for providing with financial support and material for this thesis. In particular, I would like to thank Dr. Zhou Ye, Dr. Ann-Cathrin Hellsén, BSc. Åsa Ahlin, Dr. Ola Bergman, Dr. Mats Larsson, Dr. Sven Bengtsson, Dr. Per Karlsson, Dr. Björn Skårman and MSc. Lars Hultman for their contribution to all the projects that I have been involved in. Many special thanks to everybody at the *PoP center* for helping me with all the experiments!

The Swedish Energy Agency and VINNOVA are all highly acknowledged for providing financial support for the needs of this thesis.

Urban Jelvestam, Dr. Yiming Yao and Dr. Eric Tam are all highly acknowledged for all their help and support with all the experimental work. Thank you for keeping the "machines" alive so many times, but most of all for your patience ☺ I still find your gigantic will and kindness unreal sometimes. You have my absolute respect!

I would also like to thank and acknowledge Yaroslav Kish for his contribution in this thesis with his computer programing skills and expertise.

Many special thanks to MSc. Dimitris Nikas and MSc. Daniel Castillo Gutiérrez, both of which I had the pleasure of supervising their master thesis projects. You made me so proud!

I would also like to thank all the people at the Department of Materials and Manufacturing Technology with who I had the chance to work and/or socialize with for more than five years now. This has been a big chapter in my life and you all have contributed in your own way. I wish you all the best!

Extra special thanks to Amir Malakizadi, Dr. Kumar Babu Surreddi, Dinesh Mallipeddi, Giedre Asmonaite, Dr. Seshendra Karamchedu, Dr. Carl Wadell, Johannes Erik Balatsos, Christos Doulgerakis, Sofia Poulikidou and all my good friends back in Greece which are too many to mention here! You all make me feel good about myself and that matters to me a lot!

Many super extra special thanks to the two people that I had the pleasure of sharing office with, Dr. Dimitris Chasoglou and Giulio Maistro. I don't know how it is to spend all this time during the day in a small room next to me, but if it is half of what I am suspecting it to be… then you both deserve my congratulations rather than my thanking ☺

Last but not least, I would like to dedicate this effort of mine to my family in Greece and especially to my beloved parents Nikolaos and Maria Oikonomou. I could be writing another thesis based on how much their support means to me and still it wouldn't be enough.

Thank you.

9. References

[1] Energy efficiency and specific CO2 emissions, Retrieved March 27, 2014, http://www.eea.europa.eu/data-and-maps/indicators/energy-efficiency-and-specific-co2-emissions

[2] O. Gutfleisch, M.A. Willard, E. Bruck, C.H. Chen, S.G. Sankar, J.P. Liu, *Magnetic materials and devices for the 21st century: stronger, lighter, and more energy efficient*, Advanced materials, 23, 7, (2011) 821-842.

[3] W.T. McLyman, *Transformer and Inductor Design Handbook - Fourth Edition*, Taylor and Francis Group, LLC, (2011)

[4] H. Shokrollahi, K. Janghorban, *Soft magnetic composite materials (SMCs)*, Journal of Materials Processing Technology, Vol. 189, No. 1-3, (2007) 1-12.

[5] M. Persson, P. Jansson, A.G. Jack, B.C. Mecrow, *Soft Magnetic Composite Materials - Use for Electrical Machines*, IEEE Conference Publication, No. 412, (1995), 242-246.

[6] H. Bruncková, M. Kabátová, E. Dudrová, *The effect of iron phosphate, alumina and silica coatings on the morphology of carbonyl iron particles*, Surface and Interface Analysis, Vol. 42, No. 1, (2010) 13-20.

[7] A.H. Taghvaei, H. Shokrollahi, K. Janghorban, H. Abiri, *Eddy current and total power loss separation in the iron–phosphate–polyepoxy soft magnetic composites*, Materials & Design, Vol. 30, No. 10, (2009) 3989-3995.

[8] S. Wu, A. Sun, W. Xu, Q. Zhang, F. Zhai, P. Logan, A.A. Volinsky, *Iron-based soft magnetic composites with Mn–Zn ferrite nanoparticles coating obtained by sol–gel method*, Journal of Magnetism and Magnetic Materials, Vol. 324, No. 22, (2012) 3899-3905.

[9] P. Jansson, *Processing aspects of soft magnetic composites*, Proceedings of the Euro PM2000 Conference Soft Magnetic Materials Workshop, Munich, Germany, (2000), 9-14.

[10] Y. Zhou, L. Hultman, L. Kjellen, *Production Aspects of SMC Components*, Powder Metallurgy World Congress & Exhibition, Vol. 4, (2004), 552-559.

[11] B.D. Cullity, C.D. Graham, *Introduction to Magnetic Materials, Second Edition*, IEEE Press, (2009)

[12] H. Skarrie, *Design of Powder Core Inductors*, Lund University, Sweden, (2001).

[13] Y. Zhang, M.-C. Cheng, P. Pillay, *Magnetic Characteristics and Excess Eddy Current Losses*, Proccedings IEEE Industry Applications Society Annual Meeting, (2009), 1-5.

[14] L.O. Hultman, A.G. Jack, *Soft Magnetic Composites - Materials and Applications*, Electric Machines and Drives Conference, IEMDC'03, IEEE International, Vol. 1, (2003), 516-522.

[15] ARNOLD Magnetic Technologies, Soft Magnetics Applications Guide, Retrieved March 29, 2014, http://www.arnoldmagnetics.com/Soft_Magnetics_Applications_Guide.aspx

[16] Höganäs AB. Somaloy Technology, Applications, Retrieved March 29, 2014, http://www.hoganas.com/en/Segments/Somaloy-Technology/Applications/

[17] AMES, Soft Magnetic Parts, Retrieved March 29, 2014, http://www.ames.es/products/1037-2/

[18] K. Narasimhan, F. Hanejko, M.L. Marucci, *Soft magnetic material for A.C. applications*, Hoeganes Corporation, Available from <http://www.yunamedia.com/GKNPLCHC.com/KyungHoeganae/TechPapersv2/201.pdf>.

[19] O. Larsson, *Fe-based Amorphous Powder for Soft-Magnetic Composites*, Department of Materials Science and Engineering, Royal Institute of Technology, Stockholm, Sweden, Master Thesis, (2013).

[20] C. Suryanarayana, A. Inoue, *Iron-based bulk metallic glasses*, International Materials Reviews, Vol. 58, No. 3, (2013) 131-166.
[21] O. Andersson, P. Hofecker, *Advances in Soft Magnetic Composites – Materials and Applications*, International Conference on Powder Metallurgy & Particulate Materials, PowderMet 2009, Las Vegas, Nevada, 2, (2009). ISBN: 978-0-9819496-1-1
[22] GKN Sinter Metals - Soft Magnetic PM, http://www.gkn.com/sintermetals/capabilities/soft-magnetic-pm/Pages/default.aspx
[23] P. Jansson, *Phosphate coated iron powder and method for the manufacturing thereof*, No. US 6,348,265 B1, Feb. 19, (2002)
[24] I. Hemmati, H.R.M. Hosseini, S. Miraghaei, *Effect of processing parameters on electrical,mechanical and magnetic properties of iron-resin soft magnetic composite*, Powder Metallurgy, Vol. 50, (2007) 86-90.
[25] S. Rebeyrat, J.L. Grosseau-Poussard, J.F. Dinhut, P.O. Renault, *Oxidation of phosphated iron powders*, Thin Solid Films Vol. 379, No. 1-2, (2000) 139-146.
[26] A.H. Taghvaei, H. Shokrollahi, K. Janghorban, *Properties of iron-based soft magnetic composite with iron phosphate–silane insulation coating*, Journal of Alloys and Compounds, Vol. 481, No. 1-2, (2009) 681-686.
[27] K. Ogle, M. Wolpers, *Phosphate Conversion Coatings, Corrosion: Fundamentals, Testing, and Protection*, ASM Handbook, ASM International, Vol. 13A, (2003) 712-719.
[28] R. Balasubramaniam, *On the corrosion resistance of the Delhi iron pillar*, Corrosion Science, Vol. 42, (2000) 2103-2129.
[29] D. Nikas, *Characterization of electrically insulating coatings for soft magnetic composite materials by means of surface sensitive analytical techniques*, Materials and Manufacturing Department, Chalmers University of Technology, Gothenburg, Sweden, MSc Thesis, (2013).
[30] D. Chasoglou, *Surface Characteristics of Water Atomized Pre-alloyed Steel Powders and their effect on Sintering*, Chalmers University of Technology, PhD thesis, (2012).
[31] C.D. Wagner, W.M. Riggs, L.E. Davis, J.F. Moulder, G.E. Muilenberg, *Handbook of X-ray Photelectron Spectroscopy*, Perkin-Elmer Corporations, Physical Electronics, Minesota, USA, (1979)
[32] J.F. Watts, J. Wolstenholme, *An introduction to Surface Analysis by XPS and AES*, John Wiley & Sons, Ltd, Chichester, UK, (2005) DOI:10.1002/0470867930
[33] D. Briggs, M.P. Seah, *Practical surface analysis: Auger and X-ray photoelectron spectroscopy*, Vol. 1, John Wiley and Sons Ltd, (1990)
[34] L. Nyborg, A. Nylund, I. Olefjord, *Thickness determination of oxide layers on spherically-shaped metal powders by ESCA*, Surface and Interface Analysis, Vol. 12, No. 1-12, (1988) 110-114.
[35] A.J. Schwarts, M. Kumar, B.L. Adams, *Electron Backscatter Diffraction in Materials Science*, Kluwer Academic/Plenum, New York, (2000).
[36] L.N. Brewer, M.A. Othon, L.M. Young, T.M. Angeliu, *Misorientation mapping for visualization of plastic deformation via electron back-scattered diffraction*, Microscopy and microanalysis : the official journal of Microscopy Society of America, Microbeam Analysis Society, Microscopical Society of Canada, 12, 1, (2006) 85-91.
[37] S.I. Wright, M.M. Nowell, D.P. Field, *A Review of Strain Analysis Using Electron Backscatter Diffraction*, Microscopy and Microanalysis, Vol. 17, No. 03, (2011) 316-329.
[38] T. Maitland, S. Sitzman, *Electron Backscatter Diffraction (EBSD) Technique and Materials Characterization Examples*, Scanning Microscopy for Nanotechnology: Techniques and Applications, 1st edn. Springer, New York, Chapter 2, (2006).

[39] I. de Diego-Calderón, M.J. Santofimia, J.M. Molina-Aldareguia, M.A. Monclús, I. Sabirov, *Deformation behavior of a high strength multiphase steel at macro- and micro-scales*, Materials Science and Engineering: A, 611, (2014) 201-211.
[40] C.A. Schuh, *Nanoindentation studies of materials*, Materials Today, Vol. 9, No. 5, (2006) 32-40.
[41] W.C. Oliver, G.M. Pharr, *An improved technique for determining hardness and elastic modulus using load and displacement sensing indentation experiments*, J. Mater. Res, Vol. 7, No. 6, (1992) 1564-1583.
[42] D.R. Baer, M.H. Engelhard, A.S. Lea, P. Nachimuthu, T.C. Droubay, J. Kim, B. Lee, C. Mathews, R.L. Opila, L.V. Saraf, W.F. Stickle, R.M. Wallace, B.S. Wright, *Comparison of the sputter rates of oxide films relative to the sputter rate of SiO[sub 2]*, Journal of Vacuum Science & Technology A: Vacuum, Surfaces, and Films, 28, 5, (2010) 1060.
[43] A. Ünal, *Interpretation of ESCA thickness measured on non-uniform oxide layers*, Powder Metallurgy, Vol. 34, No. 2, (1991) 135-138.
[44] M. Norell, L. Nyborg, T. Tunberg, I. Olefjord, *Thickness Determination of Surface Oxide on Metal Powder by AES Depth Profiling*, Surface and Interface Analysis, Vol. 19, (1992) 71-76.
[45] T.S.N.S. Narayanan, *Surface pretreatment by phosphate conversion coatings- a review*, Rev. Adv. Mater. Sci., 9, (2005) pp. 130-177.
[46] Y. Song, S. Yang, P. Y. Zavalij, M.S. Whittingham, *Temperature-dependent properties of FePO4 cathode materials*, Materials Research Bulletin, 37, (2002) 1249-1257.
[47] R. Brow, C. Arens, Y. X., E. Day, *An XPS study of iron phosphate glasses*, Physics and Chemistry of Glasses, 35, 3, (1994) 132-136.